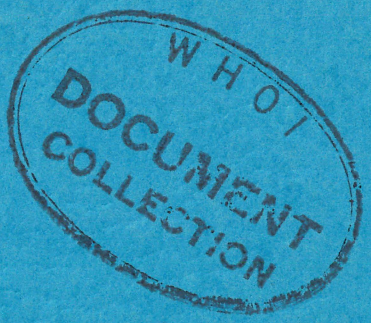

WOODS HOLE OCEANOGRAPHIC INSTITUTION

Reference No. 63-22

ON THE ESTIMATION OF THE DIRECTIONAL SPECTRUM OF OCEAN WAVES FROM TIME SERIES OBSERVATIONS OF SURFACE ELEVATIONS

WOODS HOLE, MASSACHUSETTS

Woods Hole Oceanographic Institution
Woods Hole, Massachusetts

Re written
See Ref 65-20

Reference No. 63-22

ON THE ESTIMATION OF THE DIRECTIONAL SPECTRUM OF OCEAN WAVES FROM TIME SERIES OBSERVATIONS OF SURFACE ELEVATIONS

by

Raymond G. Stevens

This research was supported in part by the Bureau of Ships Fundamental Hydromechanics Research Program, S-R009 01 01, administered by the David Taylor Model Basin.

TECHNICAL REPORT
Submitted to the Office of Naval Research Under Contract Nonr-3351(00) NR 083-501 and Nonr 2734(00) NR 083-143

June 1963

APPROVED FOR DISTRIBUTION C. O'D. Iselin

Chairman, Department of Theoretical Oceanography and Meteorology

Table of Contents

List of Figures

Acknowledgements

The author wishes to express his sincere appreciation to Professor W. J. Pierson, Jr. who originally inspired the author to undertake this work and who has provided encouragement throughout the long course of this effort. Particular thanks are also due to Dr. N. F. Barber for the many hours he has devoted to thoughtful and provocative discussions with the author.

The work was supported in large part by the Bureau of Ships Fundamental Hydromechanics Research Program S-R009 01 01 administered by the David Taylor Model Basin under the Office of Naval Research, Contract NONR 2734 (00). Continuing support has been provided through the Office of Naval Research under Contract NONR 3351 (00).

Abstract

A mathematical model, consistent with certain physical features of ocean waves may be constructed by superposition of long crested sinusoidal gravity waves. Such a model, as proposed by Pierson (1955) and Longuet-Higgins (1957), depends upon the random superposition of the component waves, so that the interpretation of ocean wave measurements must be regarded as a statistical problem.

Barber (1958) has suggested that measurement of sea surface elevation as a function of time at several points along a line array may be used to deduce the distribution of energy with regard to frequency and direction of the component gravity waves. In fact, by preserving the time relationship among the signals from several detectors in a line array, the array need not be physically rotated to examine component gravity waves coming from various directions.

After developing the physical basis and mathematical notation for a stochastic model of ocean waves the limitations and potential errors in the measurement and calculation of directional spectra from finite and discrete data are discussed.

Finally, some directional spectra calculated from measurements of wind generated waves in Buzzards Bay, Massachusetts are presented without attempting interpretation.

Chapter I The Physical Model

It is a matter of common observation that a wind blowing over the sea disturbs the sea surface causing waves to be generated. The significant forces to be considered are the pressure and drag forces exerted by the wind and the force due to gravity. Rather little detailed knowledge is available concerning the nature and magnitude of the wave generating forces exerted by the wind on the sea surface while the behavior of disturbances on a water surface under the influence of gravity have been widely studied as a mathematical exercise in hydrodynamics. It is the purpose of this chapter to discuss various aspects of wind generated waves and hydrodynamic gravity waves which relate to the formulation of a physical model of wind generated waves.

Coordinate System

Figure 1·1 illustrates the coordinate system to be used throughout this paper. The x and y axes are fixed in the still water surface of the sea and the z axis is taken positive upward. The undisturbed surface is taken to be plane, that is the curvature of the earth is neglected. Displacements along the x, y and z axes will be denoted by ξ, η, ζ (xi, eta, zeta) respectively.

At time $t = t_o$ a wind with velocity -V begins to blow uniformly over the area bounded by $\pm x'$ and $\pm y'$. The wind blows in the direction of minus y. The distance along the y axis from the upwind edge of the wind field at $y = y'$ to any point in the wind area is known as the fetch of that point.

The angle ϕ is measured positive in the clockwise direction from the positive y axis to the -y axis. The angle ϕ is measured negative in a counter clockwise direction from the positive y axis to the negative y axis.

Geometry of Sea Waves

Certain broad features of wind generated waves on the sea should be mentioned. Firstly, to an observer on board a vessel, in an area where

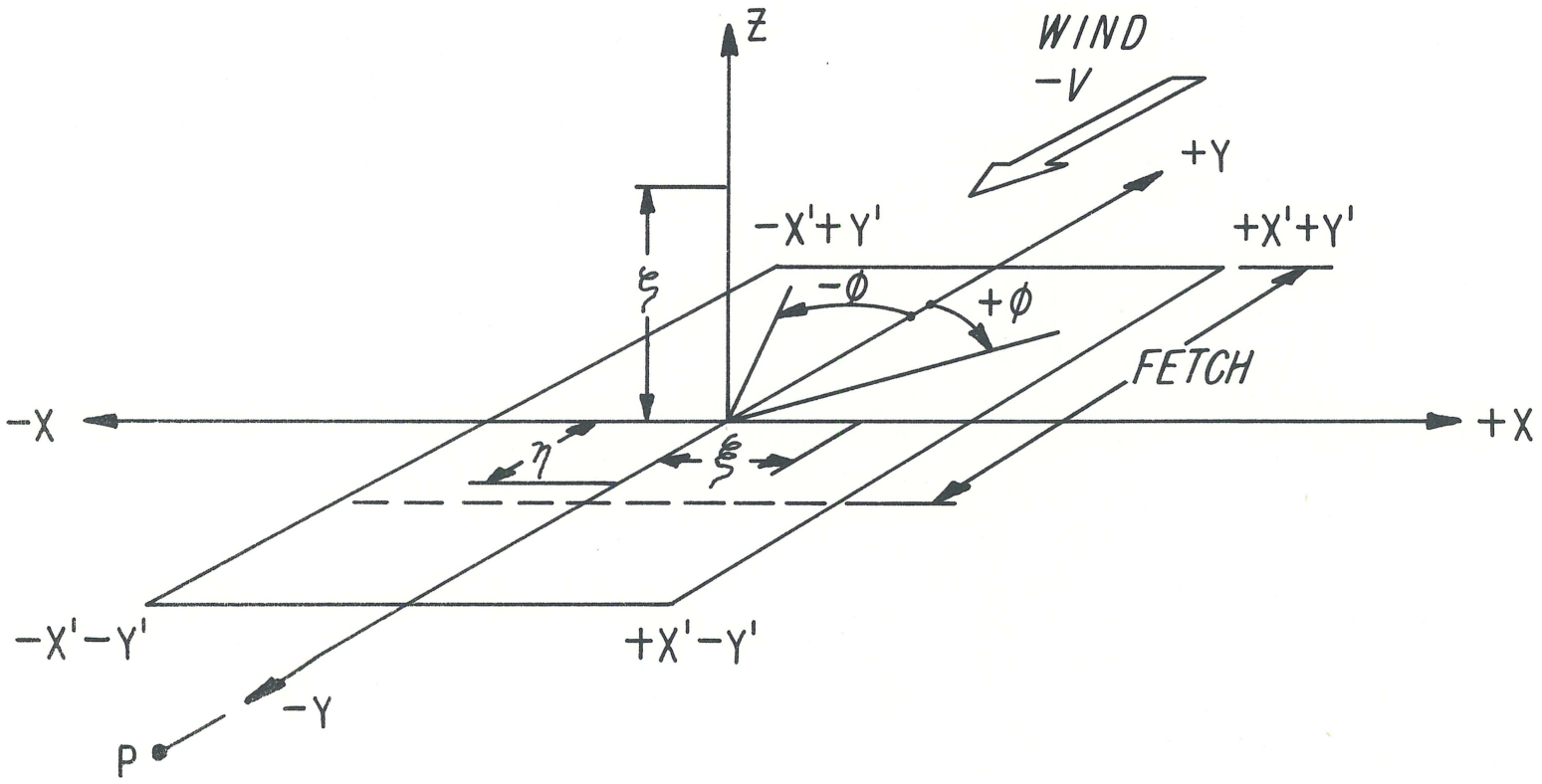

Fig. 1.1 Coordinate system

the wind is blowing the sea surface takes on a highly irregular - and sometimes violent - appearance. Sea waves have the appearance of sharp crested bumps of random size and shape. No particular shape can be associated with a sea wave profile aside from the fact that the crests are almost always steeper than the troughs and curling breakers frequently cap the waves at all wind speeds. Above some nominal wind velocity the breaking crests of the waves dissolve into patches of foam, commonly called white caps, though the breaking crests are still present at very much lower wind velocities than which white-caps appear. The horizontal extent of a particular sea wave is usually difficult to observe. When most of the sea waves appear to have a definite direction of travel it is possible to define, and visually measure, wave lengths along the direction of propagation. However, it is often quite difficult to ascribe a definite direction of travel to sea waves observed from on board a vessel.

Another geometrical feature of sea waves that does not seem to appear in the literature is the curved shape of the sea wave crests when viewed from above. It is remarkable that the nearly semicircular shape of the sea wave crests have very nearly a constant radius at any given wind speed, the radius increasing rapidly as the wind speed increases. This observation has been made repeatedly by the author from the Buzzards Bay Observing Tower which has an elevation of about 20 feet and from the Buzzards Bay Light Tower which has an elevation of about 85 feet. The circular arcs become indistinguishable from the 20 foot elevation at wind speeds above about 5 meters/sec but may be observed from the 85 foot tower at considerably higher wind speeds.

Some sort of average height of sea waves can be visually estimated by a trained observer from the air or from a surface vessel. While the height of individual waves may vary widely, the trick is to learn how to observe and average some such quantity as the height of the one-third highest of all waves observed. Extensive visual observations of this sort have been carried out, in particular by Neumann (1952). From such observations quantitative methods have been devised which relate the "height" and "length" of waves to wind speed, as discussed in Pierson, Neumann, James (1955).

The shape characteristics of sea waves are briefly described by the term irregular short crested waves.

Generation of Sea Waves

An observer on the shore of a pond can easily detect the fact that wind driven waves grow in height as they progress away from the lee shore. This is explained by assuming that wind driven waves extract momentum from the wind continuously, so long as the wave is under influence of the wind. In the case of the model shown in Figure 1·1, sometime after the wind has begun to blow uniformly over the generating area, the average wave height as measured at various places in the area can be expected to increase as the fetch increases. Furthermore, similar averages taken at a later time would all be larger than those made at the earlier time. Thus it is to be assumed that the average wave height increases as the fetch and duration increase. Of course, the sea wave height is limited, eventually, by breaking at the crests (and possibly by certain other forms of energy transfer.) Eventually, the sea waves in the area under consideration should reach a limiting height. This maximum state has been called by Neumann the "fully arisen sea." These ideas will be given more precise meaning after discussion of swell and gravity waves.

Swell Waves

The above remarks apply only to waves within the area bounded by $\pm x'$ and $\pm y'$. The term sea waves has been applied and will be consistently used in this paper to describe waves under the influence of wind. Outside the wind generating area many characteristics of wind generated waves are modified. Accordingly, waves which are no longer under the influence of the wind are called swell waves, or simply swell. The geometrical characteristics of swell are quite different from sea waves, in that the crests tend to be much less steep, breakers do not appear (so long as the swell is in deep water) and the apparent wave length and crest length of an individual swell wave is more easily observed. Swell waves are noticeably more regular and long crested than sea waves.

Some time after the wind has begun to blow, an observer located outside the generating area would detect the arrival of some low frequency, nearly sinusoidal swell waves. As time goes on the swell would lose its sinusoidal form and higher frequency wave components could be detected intermixed with the original low frequency waves.[1] On the basis of this observed behavior, Barber and Ursell (1948) proposed that swell (and sea waves) could be regarded as a superposition of gravity waves.

Gravity Waves

The term gravity waves as used in this paper will be taken to mean sinusoidal two dimensional perturbations which are supposed to exist on the surface of an ideal fluid. The properties of such waves is treated in detail by Lamb (Chap. 9), where it is also shown that an arbitrary (two dimensional) disturbance on the water surface can be represented by superposition of elementary sinusoidal gravity waves.

[1] The growing use of power spectrum analysis in oceanography has caused some chaos in the presentation of data in terms of frequency instead of periodicity. Frequency will be used throughout this paper as the wave time parameter instead of period. In order to provide a rational scale of frequency below 1 cycle per second the terms millicycle per second (mcps) and microcycle per second (μcps) are used.

The following short table, if committed to memory, serves as a useful guide in relating period to frequency.

Period (sec)	Frequency (mcps)	Frequency (μcps)
1	1,000.000	-
5	200.000	-
10	100.000	-
50	20.000	-
100 (1 min 40 sec)	10.000	-
1000 (16 min 40 sec)	1.000	1000.000
3600 (1 hr)	0.277	277.778
86,400 (1 day)	0.016	15.740

Consider a perturbation of the sea surface given by

Eq 1·1 $\zeta(x,y,t) = a \sin (kx \sin \phi + ky \cos \phi + \omega t + \beta)$

where

ζ is the surface elevation measured from the xy plane

a is the amplitude of the wave and is the maximum elevation or depression of ζ measured from the xy plane.

$\omega=2\pi f$ is a parameter with the dimensions $[T]^{-1}$. It is interpreted to be the angular frequency of the waves in time. It is measured in radians/second or milli-radians/second, while f is measured in cycles/second or millicycles/second. ω may be defined as $\omega = 2\pi/T$, where T is the time required for one complete wave cycle to pass a fixed point.

$k=2\pi/\lambda$ is a parameter with dimensions of $[L]^{-1}$. It is called the wave number. It is inversely proportioned to λ which is in turn called the wave length and is the linear distance between successive crests as measured along a line normal to the wave crests at an instant of time.

β is the angular distance between the origin of coordinates, (ie x = y = t = o) and the first wave crest. It is called the phase angle.

The form of the disturbance in space is a sinusoidal wave with parallel crests of uniform amplitude extending in the direction $\pm \phi$. Notice that the wave is defined over the entire xy plane and for all time. The crests and troughs form a fixed pattern relative to one another, but individual wave crests progress across the xy plane with a constant phase velocity given by:

1·2 $c = \omega/k$

The formulae 1·1 and 1·2 need not be restricted to water waves, but may be interpreted as simply mathematical expressions for a progressive sinusoidal wave, and so far no recourse has been made to the fact that the perturbation under consideration is a water wave. Now, the ratio ω/k is a parameter which depends upon the physics of the situation which gives rise to the waves. In the case of electromagnetic waves in a uniform medium the ratio ω/k is a constant, while for other types of waves, k and ω may be functionally related.

If it is assumed that the perturbation $\zeta(x,y,t)$ exists on the surface of an ideal (ie frictionless) fluid; that the wave amplitude and surface slope are infinitesimal; that the fluid is deep compared to the wave length and that gravity is the only important force acting on the water, then the functional relationship between k and ω is given by:

1·3 $$k(\omega) = \omega^2/g$$

and the phase velocity for deep water gravity waves becomes

1·4 $$c = g/\omega$$

The relationship between the various gravity wave parameters is given in convenient form in Table 1.

In order to simplify the notation Equation 1·1 is written

1·5 $$\zeta(x,y,t) = a \sin (lx + my + \omega t + \beta)$$

where $l = k \sin \phi$ and $m = k \cos \phi$ are respectively the x and y components of the vector wave number $\bar{k}$. The sign convention for l and m and the velocity components for waves traveling in various direction is illustrated in Figure 1·2.

According to Eq 1·4 the phase velocity is inversely proportional to the frequency. Thus, low frequency waves (long wavelengths) will propagate more rapidly than higher frequency (shorter wavelength) waves. Furthermore,

TABLE 1

Relationships Between Wave Parameters

	k	λ	ω	c	f	T
k	-	$2\pi/\lambda$ *	ω^2/g	g/c^2	$(2\pi f)^2/g$	$4\pi^2/gT^2$
λ	$2\pi/k$ *	-	$2\pi g/\omega^2$	$2\pi c^2/g$	$g/2\pi f^2$	$gT^2/2\pi$
ω	$\sqrt{gk}$	$\sqrt{2\pi g/\lambda}$	-	g/c	$2\pi f$ *	$2\pi/T$ *
c	$\sqrt{g/k}$	$\sqrt{g\lambda/2\pi}$	g/ω	ω/k **	$g/2\pi f$	$gT/2\pi$
f	$\sqrt{gk/4\pi^2}$	$\sqrt{g/2\pi\lambda}$	$\omega/2\pi$ *	$g/2\pi c$	-	$1/T$ *
T	$\sqrt{4\pi^2/gk}$	$\sqrt{2\pi\lambda/g}$	$2\pi/\omega$ *	$\frac{2\pi c}{g}$	$1/f$ *	-

k = wave number

λ = wave length

ω = angular frequency

c = phase velocity

f = frequency

T = period

* denotes a defined relationship ie independent of physics

** $c = \omega/k$ is a defined relationship but the functional relationship between k and ω must be determined by physics.

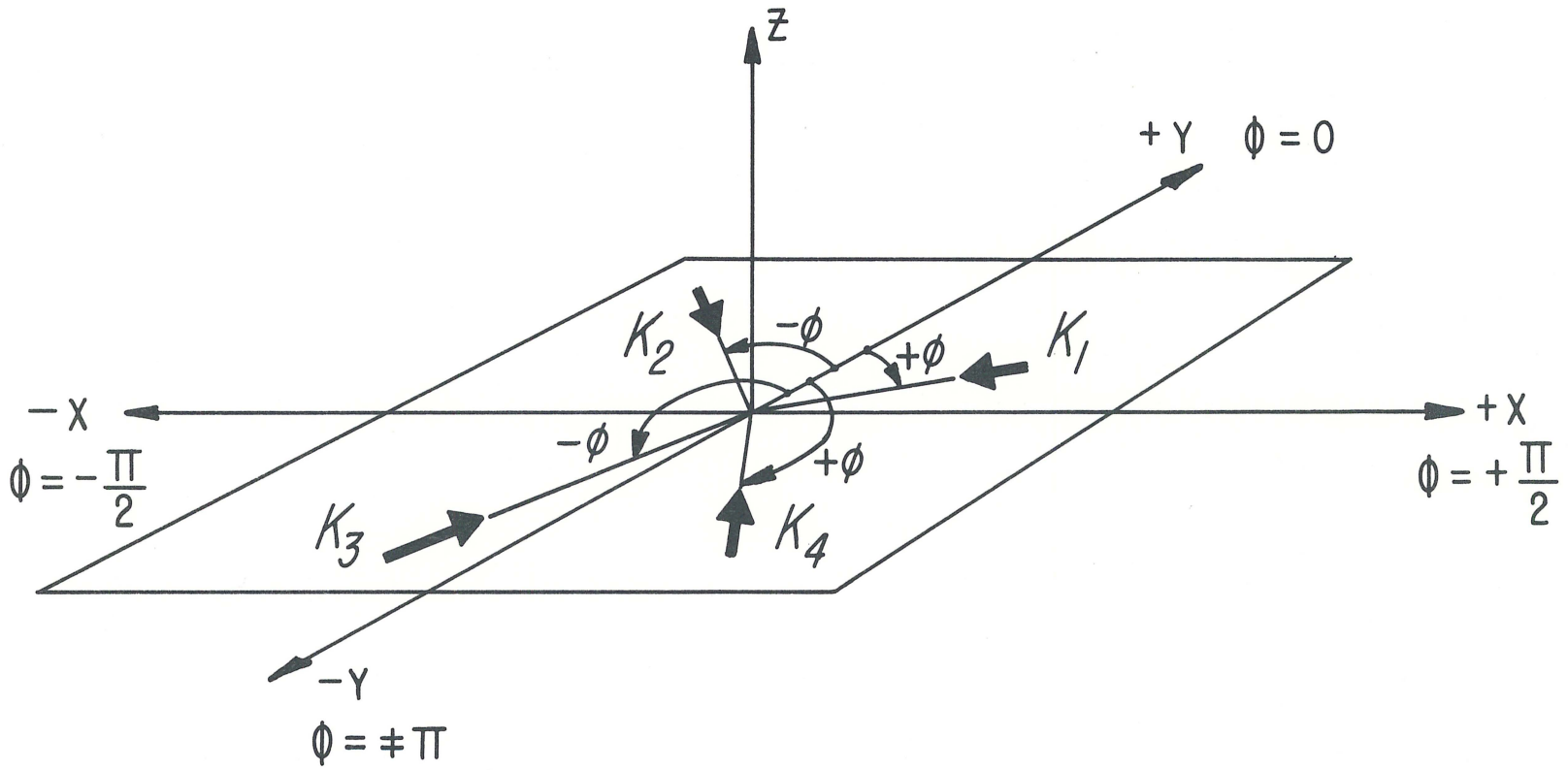

Fig. 1.2 The sign convention for waves traveling in various directions. The arrows represent wave number vectors oriented in the direction of wave travel.

a consequence of the Cauchy-Poisson wave problem (Lamb Sec 237, et seq.) is to show that an arbitrary two dimensional disturbance on the water surface can be regarded as a linear superposition of gravity waves. This implies that the disturbance would decompose into sinusoidal waves of various frequencies, each frequency propagating with its own phase velocity. The fact that swell arriving from a distant storm displays this dispersive property supports the formulation of an ocean wave model consisting of a superposition of elementary gravity waves.

The Physical Model

While it is beyond the scope and intent of the present work to formulate a detailed physical model of wind generated waves, it is essential to specify those features of the model which are relevant to the design of an observing program.

It is supposed, to begin with, that the wind blowing over the sea will cause perturbations of arbitrary shape to be generated on the sea surface. Secondly, it is assumed that this wind generated perturbation can be represented by a double superposition of gravity waves of the form given by Eq. 1·5. Thus a three dimensional perturbation is to be represented by superimposing waves traveling at various angles, ϕ, and having various frequencies ω.

Once the perturbation has been formed, it will begin to decompose into gravity waves traveling in all directions. Now, it is a common assumption in theories of wind generated waves that only those gravity waves which have velocity components in the direction of the wind are able to extract energy from the wind and increase in amplitude. Those gravity waves which do have velocity components in the direction of the wind are supposed to propagate over the surface, each frequency at its appropriate phase velocity, each wave growing in amplitude according to its ability to extract momentum from the wind. Now, a particular gravity wave train originating at a perturbation near the upwind edge of the generating area can be expected to increase its amplitude continuously,

as long as it remains under the influence of the wind, until some physical restraint operates to limit the amplitude.[2] Since the wind will form many perturbations on the sea surface an extremely complicated mixing of the gravity waves from numerous perturbations must be visualized. Gravity wave trains of the same frequency and direction but originating from different sources, may still have different phase relationships, so that when combined they may produce a reinforcement or cancellation of amplitude.

According to this model then, sea waves may be thought of as being composed of gravity wave trains of many frequencies, traveling in many directions and with many phase angles. Where these waves combine to reinforce or cancel one another a sea wave crest or trough appears. Sea waves are to be thought of then, as perturbations which are tending to disperse under the force of gravity, while at the same time the wind is acting to reinforce the perturbation.

[2]Of course, as soon as the gravity wave amplitude becomes finite the initial assumptions employed in the derivation are invalidated. Discussion of finite amplitude gravity waves is usually predicated on a non-linear reformulation of the problem [Phillips (1957) Pierson (1961)]. However it is not necessary to appeal to non-linear mathematics to see that the amplitude of gravity waves is necessarily limited. Since, in the linear case, water particles are shown to move in circular orbits under a gravity wave, and if it is required that the particles remain in the water surface, then their centrifugal acceleration must not exceed the acceleration due to gravity. This leads immediately to an expression for a maximum amplitude

$$a_{Max} = g/\omega^2 = 1/k$$

It should be remarked that this simple relationship between maximum amplitude and wave number is probably good enough to use as a rough rule of thumb for high wave numbers, but observational results and non-linear methods always yield smaller values of a_{Max}.

Certain properties of the sea waves may be deduced from the model. First of all it can be seen that since the gravity waves increase in amplitude with increasing fetch, so should the sea waves increase amplitude with increasing fetch. Another fact, apparent from the model is that at any point along a line, y = constant, the sea waves should have reached the same state of development. The dependence of sea wave height on fetch and duration is discussed in detail in Pierson, Neuman, James (1955).

These rather rough and intuitive ideas leave much to be desired in the formulation of physical model of sea waves. In particular it may be questioned whether it is justifiable to represent sea waves as a superposition of gravity when obviously forces due to the wind, as well as gravity, are operating to deform the water surface. A second point of contention may be raised regarding the suitability of superimposing two dimensional gravity waves instead of, say, gravity waves with circular symmetry. While various arguments may be made, one way or another, on these and other points, the fact remains that there is little observational evidence on which to base a realistic physical model. Therefore, these rather tentative and nebulous ideas may be conditionally accepted as the basis for planning an observational program. Hopefully, the resultant observations may be interpreted to confirm or deny these ideas or suggest others in their stead.

Chapter II The Mathematical Model

The observational program will have as its objective measurement of the amplitude of gravity wave components of the observed sea waves. The amplitude displayed as a function of frequency and direction would be called the directional amplitude spectrum, while the amplitudes displayed as a function of frequency and wave number would be called the two dimensional amplitude spectrum. However, as will be discussed, it is necessary to deal with average properties of the sea waves and, therefore, the results will be given in terms of mean square amplitudes, or "power", of the gravity wave components. The spectra will be called, respectively, the directional power spectrum, if power is shown as a function of frequency and direction, or the two dimensional power spectrum if power is given as a function of frequency and wave number.

In the next section a mathematical model of sea waves will be developed following a procedure first introduced by Pierson (1955), although the notation used here will be considerably different. The mathematical procedure consists in representing sea waves as a superposition of sinusoidal waves of all frequencies and wave numbers where the amplitudes are considered to be independent random variables. The notation is first developed for the probabilistic model where it is assumed that detailed knowledge of the sea surface elevation is available over all time and space. The effect of finite information on the calculated spectra is discussed in the following sections. The procedure for the calculation of power spectra is then developed.

It should be pointed out, however, that the methods of power spectrum analysis of random stationary time series is essentially a short-cut procedure for fourier analysis of complicated and lengthy functions. On the other hand, since the method is based on a probabilistic model, certain statistical features of the resultant spectrum can be deduced. To illustrate the procedure consider figure 2.1, which is a reproduction of two time histories of actual sea waves measured simultaneously by two detectors located only three feet apart. Quite obviously, a fourier representation of the two traces could be constructed by superimposing sinusoids. However, it is also obvious that the resultant amplitude spectra would differ markedly in detail. Of

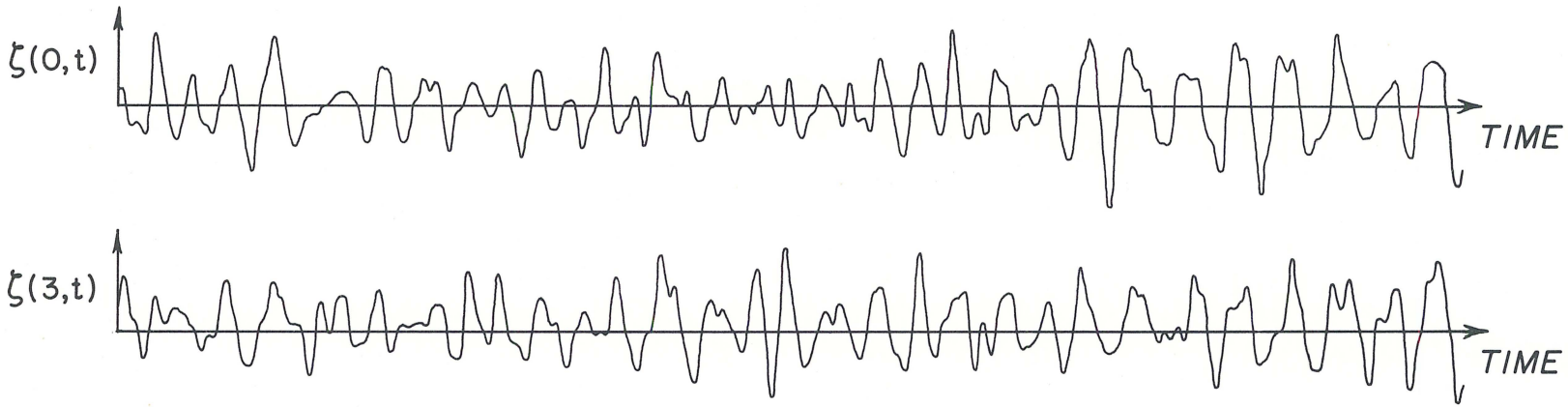

Fig. 2.1 Reproduction of two time histories of sea surface elevation taken simultaneously from detectors spaced only 3 feet apart.

course, it would be possible to collect a large number of simultaneous time histories from neighboring points on the sea surface, calculate their amplitude and find the average for each harmonic. This procedure would entail a great amount of work and, in fact, would probably be prohibitively burdensome to undertake. Fortunately, however, Pierson and Marks (1952) have shown that it is possible to employ certain methods of random noise analysis which had been developed for communication engineering in the study of sea waves. This method permits the averaging to be done first and the spectrum calculated later, thus achieving a vast economy of computation.

The Probabilistic Model of Sea Waves

In order to employ the technique of power spectrum analysis of random stationary time series, it is first necessary to formulate a probabilistic model of sea waves by superimposing a set of sinusoids in which the amplitude terms are random variables. The sinusoidal progressive waves shall be referred to as gravity waves, although no use is made of an explicit relationship between wave number and frequency until much later in the analysis. Rewriting Equation 1.5 in order to eliminate the phase angle, the equation for elementary gravity wave may be written

$$2.1 \qquad \zeta(x,y,t) = A \cos (lx + my + \omega t) + B \sin (lx + my + \omega t)$$

where $A = a\cos\beta$

$B = a\sin\beta$

Then consider a superposition of gravity waves with random amplitudes as follows:

$$2\cdot2 \qquad \zeta(x,y,t) = \int_{-\infty}^{\infty}\int_{-\infty}^{\infty}\int_{-\infty}^{\infty} \cos\,(lx + my + \omega t)\,dU(l,m,\omega) + \int_{-\infty}^{\infty}\int_{-\infty}^{\infty}\int_{-\infty}^{\infty} \sin\,(lx + my + \omega t)\,dV(l,m,\omega)$$

Here, the differential elements dU and dV contain the amplitude terms and are independent random variables. The integrals appearing in Equation 2.2 are stochastic integrals defined over a probability space, so that their interpretation differs somewhat from the usual Riemann integral. Nonetheless, any observed $\zeta(x,y,t)$ can be reproduced in detail by assigning appropriate values to dU and dV for all l,m,ω and carrying out the indicated integration.

The average value for a fluctuating signal is usually measured in terms of the amplitude squared, that is the root mean square (rms) or simply mean square, or power.[1] Consequently, what is desired is to calculate the mean square amplitude, or power, of each of the component gravity waves, directly from observations of $\zeta(x,y,t)$. Fortunately this calculation is reasonably simple so long as $\zeta(x,y,t)$ may be considered as a statistically stationary and ergodic process.

Stationarity requires only that the average properties of $\zeta(x,y,t)$ do not change radically in the observing interval. The fact that the average wave height should be constant along a line parallel to the x axis was mentioned in the discussion of the physical model. Furthermore, at some time after the wind has begun to blow the time average properties at any given point in the generating area becomes constant (fetch limited situation). Therefore, $\zeta(x,y,t)$ may be considered stationary in x and, after a suitable time lapse, stationary in t. However, in the context of the proposed physical model it is clear that the average wave height should not be considered stationary in respect to y.

[1]The mean square amplitude is often referred to as power although the use of this term does not necessarily imply a dimensional equivalence to mechanical power.

The ergodic condition provides that averages taken over a single time history of infinite extent should be equivalent to averages taken over an ensemble of finite pieces of such functions. This requirement may be met under many circumstances but it is particularly true for Gaussian processes with zero mean.

It is well to mention at this time that the statistical frequency distribution of $\zeta(x,y,t)$ is approximately Gaussian, although according to Kinsman (1960) not strictly so. While the term Gaussian is frequently associated with power spectrum analysis it is important to point out that the techniques of power spectrum analysis are not necessarily limited to processes which are closely Gaussian. In particular the Gaussian assumption is used in order to obtain precise statements concerning the reliability and variability of results, (Blackman and Tukey p.4) and has little other significance.

Covariance Function

The procedure for calculating the spectrum of the component gravity waves will be discussed first for the frequency spectrum only, in order to clarify the concepts and methods.

The first step is to form the auto-covariance function. This is done by averaging a time history of $\zeta^2(x_o,y_o,t)$. It is convenient to think of the auto-covariance function as if it were the average sea waves squared seen at the point x_o,y_o.

For the frequency spectrum then, the auto-covariance function is defined as

$$2.3 \qquad R(\tau) = \lim_{T\to\infty} \frac{1}{T} \int_{-T/2}^{T/2} \zeta(x_o,y_o,t)\cdot\zeta(x_o,y_o,t+\tau)\,dt$$

$$\equiv E\{\zeta(x_o,y_o,t)\cdot\zeta(x_o,y_o,t+\tau)\}$$

here E means expected value and may be thought of as being an average taken over time; provided $\zeta(t)$ is an ergodic process. Then from Equation 2.2

2.4 $$E\{\zeta(x_o,y_o,t)\cdot\zeta(x_o,y_o,t+\tau)\} = E\{\left[\int_{-\infty}^{\infty}\iiint \cos(lx+my+\omega t)\,dU(l,m,\omega) + \int_{-\infty}^{\infty}\iiint \sin(lx+my+\omega t)\,dV(l,m,\omega)\right] \times \left[\int_{-\infty}^{\infty}\iiint \cos(lx+my+\omega(t+\tau))\,dU(l,m,\omega) + \int_{-\infty}^{\infty}\iiint \sin(lx+my+\omega(t+\tau))\,dV(l,m,\omega)\right]\}$$

Which appears to be the average value of the product of two triple integrals! However, because of the nature of the stochastic integrals and the definition of the differential elements this is a perfectly reasonable equation. The differential elements are called orthogonal increments, in view of the independence of the random variables, and have the following properties:

$$EdU = EdV = 0$$

$$\left.\begin{aligned} &EdU(l,m,\omega)\cdot dV(l,m,\omega) = 0\\ &EdU(l,m,\omega)\cdot dU(l',\omega')\\ &EdV(l,m,\omega)\cdot dV(l',m',\omega') \end{aligned}\right\} = 0 \qquad \text{for } (l,m,\omega) \neq (l',m,\omega')$$

$$E[dU]^2 = E[dV]^2 = S(l,m,\omega)\,dl\,dm\,d\omega$$

where $S(l,m,\omega)$ is the power spectral density, or the mean square amplitude of the component gravity waves.

When the averaging process is performed on the right hand side of Equation 2.4 the cross product terms disappear and the equation reduces to:

2.5 $$E\{\zeta(x_o,y_o,t)\cdot\zeta(x_o,y_o,t+\tau)\} = \int_{-\infty}^{\infty}\iiint \cos(lx+my+\omega t)\cdot\cos(lx+my+\omega t)\,S(l,m,\omega)\,dl\,dm\,d\omega + \iiint \sin(lx+my+\omega t)\cdot\sin(lx+my+\omega(t+\tau))\,S(l,m,\omega)\,dl\,dm\,d\omega$$

When the dummy integration on dldm is performed and a trigonometric identity is used, Equation 2.5 further reduces to:

$$2.6 \qquad E\{\zeta(x_o,y_o,t)\cdot\zeta(x_o,y_o,t+\tau)\} = R(\tau) = \int_{-oo}^{oo} S(\omega)\cos\omega\tau d\omega$$

So that the covariance function and power spectrum density may be written as a fourier transform pair.

$$2.7 \qquad R(\tau) = \int_{-oo}^{oo} S(f)\cos\omega\tau df$$

$$S(f) = \int_{-oo}^{oo} R(\tau)\cos\omega\tau d\tau$$

where $\omega=2\pi f$ has been partially substituted in the equation to avoid having to carry a factor of $1/2\pi$ outside the integrals. The symbol ω is now used only as a symbol for $2\pi f$ and the frequency function is thought of in cycles, or millicycles, per second.

Two Dimensional Spectrum

In order to derive the two dimensional spectral density function $S(l,m,f)$ or the directional spectral density function $S(\phi,f)$ from measurements of surface elevation $\zeta(x,y,t)$ only, it is obviously necessary to know $\zeta(x,y,t)$ in at least two dimensions. In practice this amounts to measuring either: (1) the surface elevation over an area of sea at an instant in time, or (2) measuring the time history of the surface elevation at two or more points on the surface. The first method has actually been carried out by Pierson (1960) using stereo-photography and photogrammetry techniques, while Barber (1959) and (1962) has proposed using a kind of low frequency airborne radar which could directly measure surface elevation over fairly broad areas of the sea. Alternatively the time history of the sea surface elevation at a fixed point in space may be observed by using suitable detectors. Barber (1961) has proposed that several such detectors arranged in a line array might be used

to derive the two dimensional or directional spectrum, though it is believed that the present work is the first attempt to apply this method in practice. The two methods should lead to equivalent results, if they could be carried out to the same accuracy and provided that the actual behavior of ocean waves does not depart seriously from the proposed model of superimposed gravity waves. However, as a practical matter it is difficult to make such a comparison since the observing techniques for the two methods are not easily applied under the same circumstances.

The area observation method is ideally suited to observations over the open ocean where large waves are present and no very high degree of accuracy is required in measuring $\zeta(x,y)$. The photogrammetric technique requires the use of two aircraft and some sort of reference line of known length in the surface, and is restricted to situations that permit clear photographs to be taken from the two aircraft that form the stereo base line. Data reduction from the stereo photographs and data processing by digital computer can be a time consuming and expensive process. Barber's proposed radio diffraction technique, though it has not yet been demonstrated to work, promises to be a more efficient and highly practical means for immediately observing the ocean wave spectrum as a function of frequency and direction from a single aircraft.

Surface elevation detectors which produce a continuous signal proportional to the surface elevation at a fixed point in space can produce far more detailed and accurate measurements than the photogrammetric or radio diffraction techniques. When several such detectors are used in a line array it can be expected that details of the spectrum can be studied which would not be apparent in the area observing method. However, a serious practical problem arises when attempting to use the line array in the open ocean because of the necessity to maintain the detectors fixed in space. While various suggestions have been made for using line arrays mounted in submarines, or as a line of floats fitted with accelerometers, it appears that one appropriate application of line arrays is to gather detailed information bearing on the physical processes involved in the generation of wind waves. For this purpose a line array mounted on a fixed structure, in relatively shallow water, sheltered from the open sea

is suitable. The aim of the present work is to discuss the details of the line array method and to present some results of an observational program undertaken in Buzzards Bay, Mass.

There are at least three ways in which measurements of surface elevation along a line may be used to determine the directional spectra of ocean waves. Two of these methods require that the array be physically rotated so as to "look" in various directions and observe the power of waves of various frequencies coming from that direction. A third method permits the array to remain at a fixed orientation, preferably normal to the direction of the wind, and uses the time (ie phase) relations between the surface elevation signals as measured at various detectors, to estimate the spectrum as a function of frequency and direction. Rotatable arrays have the advantage that the computational requirements are minimized, but since the array must be rotated and stopped so as to look in various directions for a reasonable length of time, the total observing time is much longer than for the fixed array. Furthermore it is sometimes mechanically difficult to rotate the array.

Since the fixed array requires the more elaborate analysis it will be described in detail; the rotating array procedures can easily be deduced from the remaining discussion.

Cross Spectrum Analysis

Since a line array is to be used it is reasonable to locate the array along the x axis, so that y=o. In this case the <u>two dimensional spectrum density</u> $S(l,f)$ is to be found from measurement of $\zeta(x,t)$. The <u>directional spectrum density</u> $S(\phi,\omega)$ can still be determined from $S(l,f)$ since:

$$S(\phi,f)\,d\phi\,df = S(l,f)\,dl\,df$$

and $$dl = k\cos\phi\,d\phi$$

hence $$S(\phi,f) = S(l,f)\,k\cos\phi$$

Consider two surface elevation detectors placed along the x axis at location x and x + ξ. The signals from the two detectors may be considered as a two dimensional quantity and may be written in complex form as a vector:

$$2\cdot8 \quad \zeta(x,t)+i\zeta(x+\xi,t)=\int_{-\infty}^{\infty}\int \cos(lx+\omega t)\,dU(\omega,l)+\int_{-\infty}^{\infty}\int \sin(lx+\omega t)\,dV(\omega,l)$$

$$+i\left[\int_{-\infty}^{\infty}\int \cos(l(x+\xi)+\omega t)\,dV(\omega,l)+\int_{-\infty}^{\infty}\int \sin(l(x+\xi)+\omega t)\,dV(\omega,l)\right]$$

from which the complex covariance function is formed by taking the conjugate product of the vector at time t with the vector at time t+τ as indicated by:

$$2\cdot9 \quad R(\tau) = \lim_{T\to\infty} \frac{1}{T}\int_{-T/2}^{T/2} \{\zeta(x,t)+i\zeta(x+\xi,t)\}\{\zeta x,t+\tau)-i\zeta(x+\xi,t+\tau)\}dt$$

The four terms of the resultant covariance matrix are shown along with the corresponding spectral density functions in Equations 2·10. Complex notation is not carried through in these equations since it will be useful to have them displayed in real form for future development. Notice that the two cross product terms have retained their dependence on ξ and l, as was to be expected.

Equations 2·11 show the inverse fourier frequency transforms of the covariance function. The power spectrum as measured at x and at x+ξ are distinguished by the notation $S_x(f)$ and $S_\xi(f)$ respectively. Notice also that the co-spectrum $S_c(\xi,f)$ and quadrature spectrum $S_q(\xi,f)$ are formed by taking $(R_{x\xi}+R_{\xi x})/2$ and $(R_{x\xi}-R_{\xi x})/2$ which are respectively the odd and even parts of the cross product part of the covariance function.

Finally, the two dimensional spectrum is displayed explicitly by Equations 2·12. Here the odd and even parts of the two dimensional spectra are shown separately as this is the way they must be calculated. Then in Equation 2·12c they are shown combined to give the full two dimensional spectrum. Furthermore, the factor $1/2\pi$ has been eliminated from the ξ/l transform by defining

2.10

a.) $$R_{xx}(\tau) = \lim_{T\to\infty} \frac{1}{T}\int_{-T/2}^{T/2} \zeta(x,t)\cdot\zeta(x,t+\tau)dt = \int_{-\infty}^{\infty}\{\int_{-\infty}^{\infty} S(l',f)dl'\}\cos\omega\tau df$$

$$\int_{}^{T/2} \qquad\qquad \int_{}^{\infty}\int_{}^{\infty}$$

$$\ell' = \frac{\ell}{2\pi}$$

so that the use of ℓ' and ℓ in the wave number domain is analogous to the use of f and ω in the frequency domain.

The notation and conventions employed throughout this paper follow, as far as possible, the notation of Blackman and Tukey. In particular notice, that for mathematical convenience, both positive and negative frequencies are used throughout the mathematical development. However in the final computational formulae the spectral density functions will be doubled so as to conform to the physically realistic usage of positive frequencies only. It may also be remarked that, for convenience of phraseology, the mathematical model will sometimes be referred to as a superposition of gravity waves. However, no explicit use of the relationship between k and ω is made until the very end of the mathematical development.

Summary of Mathematical Model

The cospectrum and quadrature spectrum both preserve directional information and may be used to calculate the two dimensional spectrum. The procedure so far carried out is this:

1. Represent the sea surface as a random superposition of long crested sinusoidal waves.
2. Calculate the complex covariance function. The covariance function may be thought of as a time function which preserves the mean square amplitude of the original time history. Since the complex covariance function is calculated from two points separated in space it also preserves the average phase relationship of the two original time histories.
3. The fourier transforms of the elements of the covariance function show the average properties of the original time history decomposed into frequency components. Now since the phase relationship has been preserved, then at a particular frequency, f_o, the cospectrum is the mean square amplitude of the component wave which passes the two detectors in phase. The quadrature spectrum at the same f_o is the average amplitude

squared of the component wave which passes the two detectors 90° out of phase. It would be possible to combine the co and quad spectra at a given frequency to obtain an equivalent phase angle and amplitude for a single average wave, though it is not necessary to compute the phase angle directly in order to calculate the directional spectrum.

Up to this point the equations have been developed as if the time histories were known for $-\infty<t<\infty$ and as if the wave heights were known for all x. Now, in fact, a relatively few wave height detectors will be placed at discrete intervals along the axis, and the time histories will also be finite and discrete. Since truncating the information and sampling at discrete intervals both strongly affect the final analysis their effects will be considered separately and in some detail.

Finite Information

It is obvious that if unlimited information in the time domain is not available then some of the detail in the frequency domain must also be lost. The nature of the influence on the frequency spectrum caused by truncation can be seen most easily by considering the convolution of a finite function with the infinite function

Let $\zeta_1(t)$ be defined for $-\infty<t<\infty$

Let $\zeta_2(t) = 1 \qquad |t| < Tm$

$= 1/2 \qquad |t| = Tm$

$= 0 \qquad |t| > Tm$

and let

$$\zeta(t) = \zeta_1(t)\cdot\zeta_2(t)$$

The convolution theorem states that if

$S(f), S_1(f), S_2(f)$ are the fourier transforms of

$\zeta(t), \zeta_1(t), \zeta_2(t)$ respectively and if

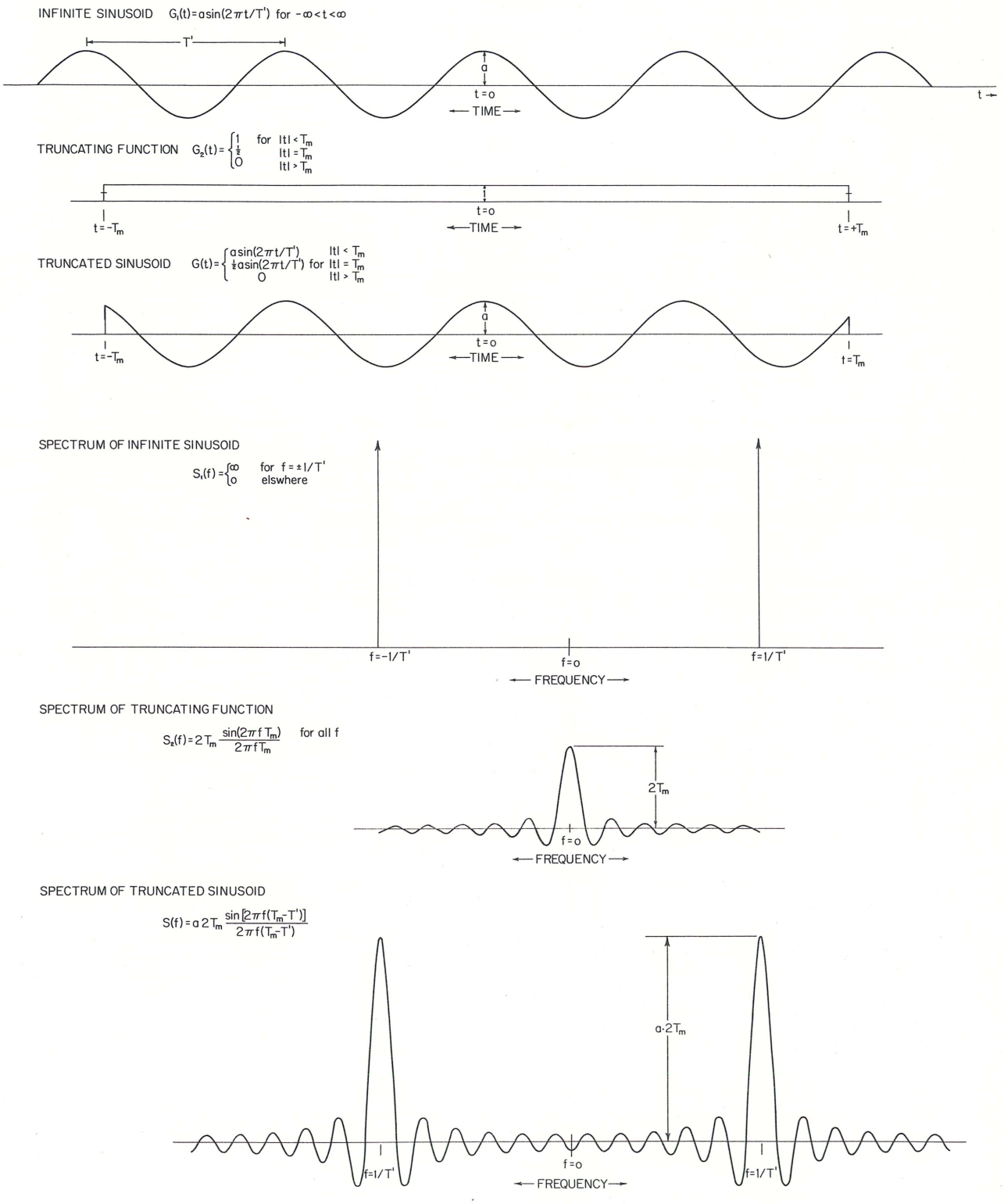

Fig. 2.2 Convolution of infinite sinusoid with truncating function.

$$\zeta(t) = \zeta_1(t) \cdot \zeta_2(t)$$

then $$S(f) = S_1(f) * S_2(f)$$

which is to be read: "S(f) is the convolution of $S_1(f)$ with $S_2(f)$." The * indicates the convolution operation. Now if $\zeta_1(t)$ is the "true" function defined for all time and if $\zeta_2(t)$ is the truncating function, then the observed function is $\zeta(t)$. Similarly if $S_1(f)$ is the spectrum of the "true" function then S(f) is the observed spectrum which is the "true" spectrum, $S_1(f)$ modified, or distorted, by the transform of the truncating function $S_2(f)$. These features are illustrated in Fig. 2·2 where the true spectrum of a simple sinusoidal wave is shown as a single line while the observed spectrum for the truncated sinusoid is shown to be spread out over the entire frequency range according to the convolution of the line f_1 with the function

$$S_2(f) = 2Tm \cdot \frac{\sin(2\pi fTm)}{2\pi fTm}$$

If the truncating function is caused to vary more smoothly instead of simply stopping abruptly at the end of the truncating interval, its fourier transform may assume a much less extreme form. By choosing appropriate shapes for the truncating function, the side lobes of the spectrum window function shown in Fig. 2·2 may be very drastically reduced, although the width of the central hump is increased. The choice of such "good shapes" has been extensively investigated for power spectrum analysis, though some controversy still prevails concerning a "good" shape for cross spectrum analysis. Regardless of what shape the truncating function or its transform finally take the important fact is that truncation of a time function causes the corresponding frequency function to be blurred and distorted.

The above remarks can be seen to apply to the ξ/1 transform as well as to the time/frequency transform. However, it is not so clear how the truncation of the time function finally affects the power spectrum. It can be shown (Blackman and Tukey p. 93) that for any truncating function applied to the time history (data window) there is an equivalent truncating function (lag window) applied to the covariance function, in the τ time domain.

In reality two things occur as a result of the truncation of the time history. Consider the estimated autocovariance function calculated from a time history of finite extent, specifically $\zeta(x,t)$ for $-Tn/2 \leq t \leq Tn/2$ as:

$$2\cdot13 \qquad \hat{R}_{xx}(\tau) = \frac{1}{Tn-|\tau|}\int_{(Tn-|\tau|)/2}^{(Tn-|\tau|)/2} \zeta(x,t)\cdot\zeta(x,t+\tau)dt$$

for $\quad |\tau| \leq Tm < Tn$

This function is only an estimate of the true autocovariance function $R_{xx}(\tau)$, and the stability of the estimate depends on the ratio Tm/Tn. That is, the longer the record, or the fewer the lags calculated, the better $\hat{R}_{xx}(\tau)$ estimates $R_{xx}(\tau)$. (Of course similar statements refer to the other elements of the cross covariance function). Thus the stability of the estimate of the cross covariance function is one effect of truncation of the time history.

The function $\hat{R}_{xx}(\tau)$ is only calculated for $|\tau| \leq Tm$; it is left undefined for $|\tau| > Tm$. Now, simply exhibiting a function of finite extent is not equivalent to truncating a function of infinite extent. Truncation implies that the function is still defined over the infinite interval but it is defined to be zero outside of the specified finite interval. Therefore the function $\hat{R}_{xx}(\tau)$ is to be truncated by a function $D_i(\tau)$ which has some special shape over the interval $|\tau| \leq Tm$ and is defined to be zero outside that range.

The function $D_i(\tau)$ is called the lag window by Blackman and Tukey. The subscript i refers to various shapes of the lag window within the interval $|\tau| \leq Tm$. The fourier transform of the lag window is denoted as $Q_i(f)$ and is called the spectrum window. Similarly, it is supposed that the time history is observed along a line segment centered at x=o and extending to $\xi = \pm L$. That is to say, the time history is observed over a finite line segment and is left undefined for $|\xi| > L$. In order to define the function for $|\xi| > L$, the spatial observations must be multiplied by a truncating function as was done in the time domain. Therefore, in order to preserve a uniformity of notation, the symbol $D_j(\xi)$ will denote the truncating function of shape j applied to the x coordinate and the corresponding fourier transform of $D_j(\xi)$ will be denoted by $Q_i(1')$ in the wave number domain.

2·14

a.) $\hat{R}_{xx}(\tau) = \frac{1}{2\theta}\int_{-\theta}^{\theta} \zeta(x,t)\cdot\zeta(x,t+\tau)dt = \int_{-\infty}^{\infty}\{\int_{-\infty}^{\infty}\hat{S}(l',f)dl'\}\cos\ \omega\tau d\tau$

b.) $\hat{R}_{\xi\xi}(\tau) = \frac{1}{2\theta}\int_{-\theta}^{\theta} \zeta(x+\xi,t)\cdot\zeta(x+\xi,t+\tau)dt = \int_{-\infty}^{\infty}\{\int_{-\infty}^{\infty}\hat{S}(l',f)dl'\}\cos\ \omega\tau d\tau$

c.) $\hat{R}_{x\xi}(\tau) = \frac{1}{2\theta}\int_{-\theta}^{\theta} \zeta(x,t)\cdot\zeta(x+\xi,t+\tau)dt = \int_{-\infty}^{\infty}\int_{-\infty}^{\infty}\hat{S}(l',f)\cos\ (\xi l-\omega\tau)dl'df$

d.) $\hat{R}_{\xi x}(\tau) = \frac{1}{2\theta}\int_{-\theta}^{\theta} \zeta(x+\xi,t)\cdot\zeta(x,t+\tau)dt = \int_{-\infty}^{\infty}\int_{-\infty}^{\infty}\hat{S}(l',f)\cos\ \xi l+\omega\tau)dl'df$

where $|t| \leq T_n$

$|\tau| \leq T_m < T_n$

$\theta = (T_n-|\tau|)/2$

2·15

a.) $\hat{S}_x(f) * Q_i(f) = Q_i(f)*\int_{-\infty}^{\infty}\hat{S}(l',f)dl' = \int_{-\infty}^{\infty}\hat{R}_{xx}(\tau)\cdot D_i(\tau)\cdot\cos\ \omega\tau d\tau$

b.) $\hat{S}_\xi(f)*Q_i(f) = Q_i(f)*\int_{-\infty}^{\infty}\hat{S}(l',f)dl' = \int_{-\infty}^{\infty}\hat{R}_{\xi\xi}(\tau)\cdot D_i(\tau)\cdot\cos\ \omega\tau d\tau$

c.) $\hat{S}_c(\xi,f)*Q_i(f) = Q_i(f)*\int_{-\infty}^{\infty}\hat{S}(l',f)\cos\ \xi l dl' = \int_{-\infty}^{\infty} 1/2\ (\hat{R}_{x\xi}(\tau)+\hat{R}_{\xi x}(\tau))\cdot D_i(\tau)\cdot\cos\ \omega\tau d\tau$

d.) $\hat{S}_q(\xi,f)*Q_i(f) = Q_i(f)*\int_{-\infty}^{\infty}\hat{S}(l',f)\sin\ \xi l dl' = \int_{-\infty}^{\infty} 1/2\ (\hat{R}_{x\xi}(\tau)-\hat{R}_{\xi x}(\tau)\cdot D_i(\tau)\cdot\sin\ \omega\tau d\tau$

2·16

a.) $\hat{S}_{ev}(l',f)*Q_i(f)*Q_j(l') = \int_{-\infty}^{\infty}\hat{S}_c(\xi,f)\cdot D_j(\xi)\cdot\cos\ \xi l d\xi = \int_{-\infty}^{\infty}\{\int_{-\infty}^{\infty} 1/2\ (\hat{R}_{x\xi}(\tau)+\hat{R}_{\xi x}(\tau))\cdot D_i(\tau)\cdot\cos\ \omega\tau d\tau\}\cdot D_j(\xi)\cdot\cos\ \xi l d\xi$

b.) $\hat{S}_{od}(l',f)*Q_i(f)*Q_j(l') = \int_{-\infty}^{\infty}\hat{S}_q(\xi,f)\cdot D_j(\xi)\cdot\cos\ \xi l d\xi = \int_{-\infty}^{\infty}\{\int_{-\infty}^{\infty} 1/2\ (\hat{R}_{x\xi}(\tau)-\hat{R}_{\xi x}(\tau)\cdot D_i(\tau)\cdot\sin\ \omega\tau d\tau\}\cdot D_j(\xi)\cdot\sin\ \xi l d\xi$

c.) $\hat{S}(l',f)*Q_i(f)*Q_j(l') = (\hat{S}_{ev}(l',f)+\hat{S}_{od}(l',f))*Q_i(f)*Q_j(l')$ for $-\infty < l' < \infty$

where $D_i(\tau) = 0 \qquad |\tau| > T_m$

$D_j(\xi) = 0 \qquad |\xi| > L$

To summarize then, estimates of the elements of the complex covariance function are to be calculated from a finite time history. These estimates will be denoted by a circumflex (e.g. $\hat{R}_{xx}(\tau)$, $\hat{R}_{\xi\xi}(\tau)$, $\hat{R}_{x\xi}(\xi,\tau)$, $\hat{R}_{\xi x}(\xi,\tau)$). The covariance functions are then to be truncated by the functions $D_i(\tau)$, and $D_j(\xi)$. The blurring and distortion of the spectrum result from the truncation of the cross covariance function, the statistical instability of the spectral estimates results from the truncation of the time history.

The equations 2·14 through 2·16 show the effect of time and space truncation. The truncating functions and their fourier transforms are shown explicitly, instead of introducing new symbols, in order to illustrate the essential nature of the blurring and distortion of the "true" spectrum. In addition, the circumflex is used to indicate that statistical estimation has occurred due to truncation of the time history.

Sampled, finite data

Before discussing the effect of sampling the data at discrete intervals it is worthwhile to mention that while it is possible to construct electrical, mechanical or optical devices to carry out the analysis from continuous data, as described so far, it is frequently desirable to carry out the analysis on discrete sampled data using a high speed digital computer. Even though it may be possible to construct a special purpose device which can carry out analysis of limited types of data, the accuracy of such machines is generally limited by close mechanical and electrical tolerances; a specific machine will operate only over a rather narrow range of frequencies, and it is usually difficult to perform any type of preliminary data conditioning, such as rejection filtering, pre-whitening or non-linear scale factor correction. It may be feasible to construct a special purpose machine when a great deal of one type of data has to be processed, and when all the characteristics of the data, and all the requirements of the problem are known in advance. Barber (1961a) has described several machines for such applications.

On the other hand, digital computers can perform spectrum analysis over a very broad range of frequencies with little or no change to the computer program. They are capable of preconditioning data in extremely

complex and subtle ways with relatively little programming and, in the more modern computers, the analysis may be performed at comparable speeds to the analogue machines. However, there is one serious problem attendant upon use of digital computers that must not be neglected. The problem is not in the computer itself, but is inherent in the process of sampling data. J. W. Tukey has named this effect "aliasing", since the result of sampling is to cause the high frequency components to adopt the name and identification of lower frequency components. While excellent discussions of this subject are given by Blackman and Tukey, Hamming (1962) and Bendat (1958) a simple demonstration will be given here after developing the equations for two dimensional spectrum analysis in the discrete parameter form.

Using the truncated power spectrum, Equation 2·14a, as an example write:

$$2\cdot17 \qquad \hat{S}_x(f)*Q_i(f) = \int_{-\infty}^{\infty} \hat{R}_{xx}(\tau)\cdot D_i(\tau)\cos\,\omega\tau d\tau = \frac{1}{Tm}\int_{-Tm/2}^{Tm/2} \hat{R}_{xx}(\tau)\cdot D_i(\tau)\cos\,\omega\tau d\tau$$

where $|\tau| \leq Tm < Tn$, and Tn is the record length. Assume that the time history $\zeta(x,t)$ has been observed at equally spaced time increments $t=0, \Delta t, 2\Delta t \ldots n\Delta t \ldots N\Delta t$ and the autocovariance function computed at equi-spaced intervals of the same duration $\tau=0, \Delta\tau, 2\Delta\tau \ldots p\Delta\tau \ldots m\Delta\tau = Tm < Tn$

Then, evaluating the rightmost integral of Equation 2·17 at the points

$$\tau = p\,\frac{Tm}{m} \qquad (=p\Delta t)$$

and at the same time writing the integral as a half range integral.

$$2\cdot18 \qquad \hat{S}_x(f)*Q_i(f) \cong 2\int_0^m \hat{R}_{xx}(p)\cdot D_i(p)\cdot \cos\left(p\,\frac{Tm}{m}\,\omega\right) d\left(p\,\frac{Tm}{m}\right)$$

for which the approximating sum is

$$\hat{S}_x(f)*Q_i(f) \cong \Delta\tau\left\{\hat{R}_{xx}(o)\cdot D_i(o) + 2\sum_{p=1}^{m-1} \hat{R}_{xx}(p)\cdot D_i(p)\cos\left(\frac{pTm\cdot\omega}{m}\right) + \hat{R}_{xx}(m) D_i(m)\cos\left(Tm\cdot\omega\right)\right\}$$

Now let $f = \frac{h}{2Tm}$ $\qquad h = 0, 1, 2, \ldots\ldots\ldots H$

$\omega = \frac{\pi h}{Tm}$

then the approximating sum becomes finally

$$2.19 \qquad \hat{S}_x(h)*Q_i(h) = \Delta\tau\{\hat{R}_{xx}(o)\cdot D_i(o)+2\sum_{p=1}^{m-1}\hat{R}_{xx}(p)\cdot D_i(p)\cos\frac{\pi ph}{m} + \hat{R}_{xx}(m)D_i(m)\cos\pi h\}$$

Now, suppose that $h = m+n$, for $n = 0, 1, 2, \ldots.$, then for the cosine term in the summation

$$\cos\frac{\pi p}{m}(m+n) = \cos\pi p\cos\frac{\pi pn}{m} - \sin\pi p\sin\frac{\pi pn}{m} = \pm\cos\frac{\pi pn}{m}$$

and since n and h are both integers $\cos\frac{\pi pn}{m}$ is indistinguishable from its <u>alias</u> $\cos\frac{\pi ph}{m}$. Thus it is clear that frequencies higher than $f = m/2Tm$ will appear somewhere in the range

$$-1/2\Delta t \leq f \leq 1/2\Delta t$$

It is also apparent that once the sampling interval Δt is chosen, the sampled data <u>is aliased</u> and nothing whatsoever can be done to recover the true identity of the high frequency components.

Naturally, if the amplitude, or power, of the high frequency aliased components is small, little damage is done to the final spectrum. But if there are high frequency components with substantial power present they will be aliased regardless of whether they hold any interest to the investigator or not. Fortunately, naturally occurring phenomena tend to fall into frequency domains within which the high frequencies become rapidly attenuated within a domain, and the next higher frequency domain usually begins with lower power components.

In the practical situation, a further fortunate circumstance arises from the fact that most transducers which can be used to sense physical variables attenuate the higher frequency components. In fact, if high fre-

quency energy is likely to contaminate a sampled time history by aliasing, the only means of preventing this occurrence is to incorporate a low pass filter into the transducer, or other portion of the data acquisition system prior to sampling.

All of the above remarks, except possibly those pertaining to low pass filters, apply equally well to sampling in the space coordinate. However, some special considerations apply to the space samples since the space parameter k and the time parameter ω are functionally related.

Assume that the truncated cross covariance function has been observed over the line sector $-L \leq \xi \leq L$ at the points

$$\xi = 0, \Delta\xi, 2\Delta\xi, \ldots\ldots\ldots, r\Delta\xi\ldots\ldots\ldots, R\Delta\xi \qquad R\Delta\xi = L$$

then the first integral on the right of equation 2·16a may be written as a half range integral over ξ, and evaluated at the points

$$\xi = r\frac{L}{R} \qquad r = 0, 1, 2, \ldots R$$

for which the approximating sum is

$$\hat{S}_{ev}(1',f)*Q_i(f)*Q_j(1') \tilde{=} \Delta\xi \left\{\hat{S}_c(o,f)\cdot D_j(o)+2\sum_{r=1}^{R-1}\hat{S}_c(r,f)\cdot D_j(r)\cos\frac{rL1}{R} + \hat{S}_c(R,f)\cos L1\right\}$$

Now let $\quad 1' = q/2\cdot L \qquad$ for $q = 0, 1, 2 \ldots. Q$

$$1 = \pi q/L$$

Then by a similar argument to the one presented for frequency aliasing it can be shown that wave numbers greater than $|1'| = R/2L$ will be aliased into the range

$$-1/2\Delta\xi < 1' < 1/2\Delta\xi$$

Hence the approximating sum may be written

$$\hat{S}_{ev}(1',f)*Q_i(f)*Q_j(q) \cong \Delta\xi \left\{\hat{S}_c(o,f)\cdot D_j(o)+2\sum_{r=1}^{R-1}\hat{S}_c(r,f)\cdot D_j(r)\cos\frac{\pi rq}{R} + \hat{S}_c(R,f)D_j(r)\cos \pi q\right\}$$

for $q = 0 \pm 1, \pm 2, \ldots \pm R$

Sampling in the time domain produces a maximum non-aliased frequency, called the Nyquist, or folding, frequency which is given by

2·20 $$f_N = 1/2\Delta t$$

In the space domain it is also necessary to choose $\Delta\xi$, the space sampling interval, small enough so that aliasing is not important. Here, the comparable quantity to frequency is the wave number, k, so that analogous to Equation 2·20 the folding wave number may be given by

2·21 $$k_N/2\pi = k'_N = 1/2\Delta\xi$$

Up to this point no use has been made of a specific functional relationship between k and ω. However, it is apparent that since k and ω are functionally related, the choice of Δt will influence the choice of $\Delta\xi$. Specifically if it is assumed that

$$k = \omega^2/g$$

it follows that

$$k'_N = 1/2\Delta\xi = \pi/2g(\Delta t)^2$$

which requires that

2·22 $$\Delta\xi \leq g(\Delta t)^2/\pi = g/4\pi f_N^2$$

Thus, having chosen a time sampling interval Δt, with due consideration of aliasing, the space sampling interval $\Delta\xi$ must be chosen to be commensurate with Δt, according to the relationship assumed between k and ω.

The finite, discrete cross covariance estimates are given by Equations 2·23, while the formulae for the finite discrete cross spectrum estimates are given by Equations 2·24. The formulae for the two dimensional spectral densities in terms of 1' are given by Equations 2·25. It would be possible to write Equations 2·25a and 2·25b as a double summation over time lag (p) and space interval (r) but the resultant lengthy expressions are not given since they have little practical value. Actual calculation of the two dimensional spectral densities is carried out by first calculating the frequency cross spectral densities and then taking the spatial fourier transform.

Again, the time and space truncations are indicated by the truncating functions $D_i(p)$, $D_j(r)$ and their respective fourier transforms $Q_i(h)$ and $Q_j(q)$, with the circumflex indicating truncation of the time history. Also, the discrete parameters q, and h serve to indicate that the spectral estimates are aliased estimates of the true spectrum. Thus the notation, while cumbersome, serves to demonstrate the fact that the calculated spectral densities are blurred, distorted, aliased estimates of a "true" spectral density.

2.23

a.) $\hat{R}_{xx}(p) = \frac{1}{N-p} \sum_{n=1}^{N-p} \zeta_n(x) \cdot \zeta_{n+p}(x)$

b.) $\hat{R}_{\xi\xi}(p) = \frac{1}{N-p} \sum_{n=1}^{N-p} \zeta_n(x+\xi) \cdot \zeta_{n+p}(x+\xi)$

c.) $\hat{R}_{x\xi}(p) = \frac{1}{N-p} \sum_{n=1}^{N-p} \zeta_n(x) \cdot \zeta_{n+p}(x+\xi)$

d.) $\hat{R}_{\xi x}(p) = \frac{1}{N-p} \sum_{n=1}^{N-p} \zeta_n(x+\xi) \cdot \zeta_{n+p}(x)$

2.24

a.) $\hat{S}_x(h) * Q_i(h) = 2\Delta\tau \{ \sum_{p=o}^{m} R_{xx}(p) \cdot D_i(p) \cdot \delta(p) \cdot \cos \frac{\pi p h}{m} \}$

b.) $\hat{S}_\xi(h) * Q_i(h) = 2\Delta\tau \{ \sum_{}^{m} R_{\xi\xi}(p) \cdot D_i(p) \cdot \delta(p) \cdot \cos \frac{\pi p h}{m} \}$

d.) $\hat{S}_q(\xi,h) * Q_i(h) = \Delta\tau \{ \sum_{p=1}^{m-1} [R_{x\xi}(p) - R_{\xi x}(p)] \cdot D_i(p) \cdot \sin \frac{\pi p h}{m} \}$

2.25

a.) $\hat{S}_{ev}(q,h) * Q_i(h) * Q_j(q) = 2\Delta\xi \{ \sum_{r=o}^{R} \hat{S}_c(r,h) * Q_i(h) \cdot D_j(r) \cdot \delta(r) \cos \frac{\pi r q}{R} \}$

b.) $\hat{S}_{od}(q,h) * Q_i(h) * Q_j(q) = \Delta\xi \{ \sum_{r=o}^{R-1} \hat{S}_q(r,h) * Q(h) \cdot D_j(r) \sin \frac{\pi r q}{R} \}$

c.) $\hat{S}(q,h) * Q_i(h) * Q_j(q) = [\hat{S}_{ev}(q,h) + \hat{S}_{od}(q,h)] * Q_i(h) * Q_j(q)$ for $-R < q < R$

$\delta(p) = \{ {1 \atop 1/2}$ $p=1,2,\ldots m-1$; $p=o,m$

$\delta(r) = \{ {1 \atop 1/2}$ $r=1,2,\ldots r-1$; $r=o,R$

$T_m = m\Delta t$

$L = R\Delta\xi$

$f_h = h/2\Delta t \cdot m$ for $h = -m,\ldots, -1, 0, 1, 2, \ldots m$

$1'_q = q/2\Delta\xi \cdot R$ for $q = -R,\ldots, -1, 0, 1, 2, \ldots R$

Chapter III Directional Spectrum

Since the final result of this work is intended to be the practical calculation of directional gravity wave spectra, various refinements and modifications must be made to the equations developed so far. In this chapter a variety of topics will be treated, with no particular continuity between the various sections, and, finally, equations suitable for calculation of the directional wave spectrum will be presented.

Before proceeding with the mathematical development it is worth while to consider some of the physical aspects involved in measuring the directional spectrum. To start with, the model supposes that sea waves may be considered to be a superposition of a great many sinusoidal waves of various frequencies, which are propogating over the surface in various directions at speeds appropriate to gravity waves. The troughs and crests of each component wave train are assumed to be of unlimited extent in the direction normal to their propogation, so that each crest, say, of every component wave will pass under all the detectors of the array sooner or later. The crest of a component wave which is moving normal to the array will, of course, pass under all detectors simultaneously, while a given crest for a component wave moving at an angle to the array will pass each detector in sequence. The time interval which elapses while a particular crest passes from one detector to another depends upon the speed of propogation of the wave train, the angle which the wave front makes with this array and the distance between detectors. On the other hand, the time between passages of successive crests of the same component wave at any one detector will be constant regardless of the direction of propogation of the wave train.

The procedure for measuring the directional spectrum of sea waves is somewhat analogous to radio direction finding. The radio receiver is first tuned to a fixed frequency and then the antenna is rotated to find the direction of maximum signal strength. Maximum signal strength occurs when the wave fronts are parallel to the antenna, so that the signals from all the detectors are in phase and act to reinforce each other. In the present case, however, there is no single direction of maximum signal to be expected and furthermore, the array is not actually to be rotated. Virtual, or apparent, rotation of the array could be achieved by delaying the signals from the various elements of the array so that a wave front arriving from a fixed direction would be apparently in phase at each detector. The amount of delay

between detectors in the array would depend upon the distance between detectors and the phase velocity appropriate to the frequency being examined. The signal delaying procedure as described here could actually be performed in the time domain. However, it is much simpler to perform the equivalent operations in the frequency domain after the co and quadrature spectra are computed, though it is more difficult to explain the physical process in terms of operations in the frequency domain.

Resolution and Distortion

As was briefly pointed out in the last chapter the effect of finite information in the time and space domain is to cause a blurring and distortion in the frequency and wave number domain. The following discussion is intended to clarify these matters in the particular context of this paper although excellent discussions are available elsewhere. (In particular see Guillemin (p. 485)). The following nomenclature will be adopted: the truncating function $D_i(\tau)$, is called the lag window and its fourier transform $Q_1(f)$ is called, the spectral window. These expressions are identical in form to the truncating function $D_j(\xi)$ which is called the array weighting function, and its fourier transform $Q_j(1^\circ)$, which is called the array pattern and $Q_j(\phi)$ which is called the array directional pattern.

It was pointed out in the last chapter that if the time observations were abruptly terminated the resultant spectrum would be blurred and distorted according to its convolution with the function

$$3.1 \qquad Q_o(f) = 2Tm \frac{\sin 2\pi fTm}{2\pi fTm}$$

In the space/wave number domain this becomes

$$3.2 \qquad Q_o(1^\circ) = 2L \frac{\sin 2\pi 1^\circ L}{2\pi 1^\circ L}$$

where 2L is the length of the observing array and

$$1^\circ = L/2\pi$$

the function is illustrated in Figure 3·1.

From the figure it can be seen that the width of the central maximum, or main lobe, is given by

3·3 $$W_o(1') = \frac{1}{L} = \frac{1}{\Delta\xi \cdot R}$$

or $$W_o(f) = \frac{1}{Tm} = \frac{1}{\Delta t \cdot m}$$

the remaining lobes are of width $W_o/2$.

The height of the main lobe is

3·4 $$Q_o(1')=2L$$

at $1' = o$

$$Q_o(f)=2Tm$$

at $f = o$

while the ratio of the side lobe height to the height of the main lobe is given by

3·5 $$\frac{\text{Side lobe height}}{\text{Main lobe height}} = \frac{(-1)^n \cdot 2}{(2n-1)\pi} \qquad \text{for } n = 1, 2, \ldots$$

The effect of the convolution can be interpreted as follows. Suppose that it is desired to observe the two dimensional spectral density $S(1',f)$ at the single frequency f_1 and at wave number $1'_1$. Then because of the finite extent of time and space observations the observed spectral density will be

$$S(1',f)*Q_o(f_1)*Q_o(1'_1)$$

which means that the entire spectral density function $S(1',f)$, will be observed for all f and $1'$ with the various spectral components attenuated by the spectral window $Q_o(f_1)$ and array pattern $Q_o(1'_1)$.

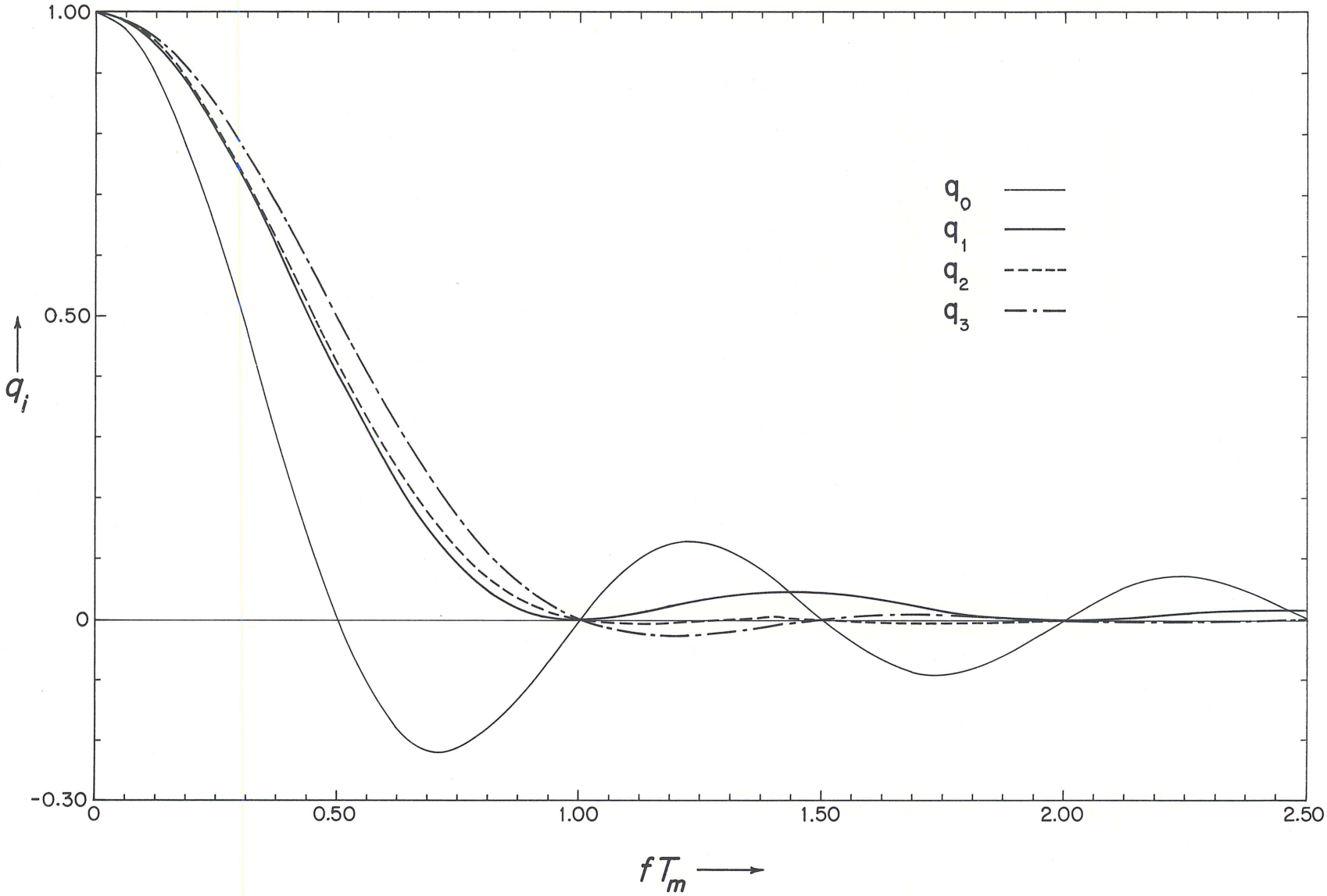

Fig. 3.1 Some truncating functions and their spectral windows or array patterns.

If it were possible to produce ideal functions $Q_I(f)$ and $Q_I(1')$ which had rectangular shaped main lobes of infinitesimal width and no side lobes, these functions would trace out the true spectral density function in exact detail. Now, while it is not possible to attain this ideal it is possible to achieve certain more desirable characteristics. First, however, the distinction between resolution and distortion should be clarified. Consider for example a spectral window and array pattern, which have a single rectangular shaped lobe of finite width and no side lobes. These functions would produce an observed spectral density function which would be blurred but not distorted. That is to say, at any given frequency f_1 and wave number $1'_1$, the observed spectral density $S(1'_1,f)$ would in fact include the spectral components in the range $f_1 \pm W/2$ and $1'_1 \pm W/2$ but these components would be uniformly weighted. Hence the spectrum would be blurred, that is the resolution would be limited by the width of the main lobe. It seems reasonable therefore to specify the resolution of the functions $Q_i(f)$ and $Q_j(1')$ by the width of the main lobe, and in some way to specify the distortion in terms of the departure of the function from the ideal rectangular shape.

It is convenient to adopt the nomenclature employed in radio antenna design where the resolving power is defined as the reciprocal of the beam width. In the present case it would be suitable to define

$$\text{Resolving Power} = RP_i = \frac{1}{W_i}$$

where i refers to the shape as in $Q_i(1')$, $D_i(\xi)$. In which case the resolving power for $Q_o(1')$ is given by

$$RP_o(1') = \frac{1}{W_o} = L$$

However, there is always some problem in interpreting the observed spectrum. Suppose for instance that using the spectral window $Q_o(f)$ a spectrum of the exact shape of $Q_o(f_1)$ is observed. That is, the observed spectrum appears to have a ratio of side lobe height to main lobe height corresponding to Equations 3·3 and 3·5, centered at frequency f_1. Now, of

course such a result could occur if the true power spectrum actually consisted of a single line, that is, if only the single frequency, f_1, were present. However, an important result given by Blackman and Tukey (p. 18) shows that if the signal amplitudes followed a Gaussian distribution and if the true power spectrum was rectangular in form, centered at frequency f_1 and extending over the range $f = f_1 \pm 1/4$ Tm then the same spectrum would be observed. In other words, the $Q_o(f)$ spectral window can not distinguish between a single frequency and a rectangular spectrum half the width of its main lobe, provided that the signal source for the rectangular spectrum is Gaussian. The same results may be extended to the array pattern in the wave number coordinates.

Blackman and Tukey discuss the resolving power of various spectral windows in terms of an equivalent width of the main lobe, which may be interpreted to be the width of the largest rectangular spectrum, arising from a Gaussian signal, that could produce an observed spectrum identical to the spectral window. Resolving power may be defined in terms of this reduced, or equivalent width, of the array pattern, or spectral window, so that the equivalent resolving power may be defined as

$$ERP_i = \frac{1}{W_{ei}}$$

where again the subscript i refers to a particular shape of spectral window or array pattern. For $Q_o(f)$ the equivalent resolving power is

3.6a $\quad ERP_o(f) = 2Tm$

while for $Q_o(1')$

3.6b $\quad ERP_o(1') = 2L$

If the above results are viewed in somewhat different perspective it can be seen that if the true power spectrum of a Gaussian signal is essentially constant over a fairly wide range of frequency or wave number and if the spectrum is calculated at intervals of one half the main lobe

width of $Q_o(f)$ and $Q_o(l')$ then each estimate covers a distinct, non-overlapping range of frequency and wave number. Thus for $Q_o(f)$ and $Q_o(\xi)$ adjacent spectral estimates may be considered to be independent estimates if they are calculated at increments

$$\Delta f = Tm/2$$

$$\Delta l' = L/2$$

which are seen to be precisely the intervals chosen for calculating the discrete two dimensional spectral densities given by equations 2.24 and 2.25.

The only method for improving resolution, that is of reducing the width of the main lobe, is to increase the duration of the observations, as is clearly shown by Equation 3.3. On the other hand, distortion may be reduced by causing the truncating function to vary more smoothly over its range instead of simply terminating abruptly. Unfortunately, an improvement of shape of the main lobe, or reduction of side lobe heights is achieved only at the expense of increasing the main lobe width. Thus, efforts to reduce distortion of the observed spectrum causes a further decrease in resolving power.

The characteristics of various spectral windows have been extensively discussed. Blackman and Tukey from whom the present nomenclature has been adopted, discuss five types of lag windows with their corresponding spectral windows, denoted as $D_i(\tau)$ and $Q_i(f)$ $i = 0, 1, 2, 3, 4$. Some of these are illustrated in figure 3.1 along with their mathematical specifications. The functions $i = 2$ and $i = 3$ known as "hanning" and "hamming" respectively, have been extensively used in the past becuase of their computational simplicity. Parzen (1957) has developed a more ideally shaped spectral window which does not have the advantage of computational simplicity while the methods due to Lanczos (see Hamming p. 297) also do not retain the computational simplicity of hanning and hamming. The width of the main lobe of $Q_2(f)$ and $Q_3(f)$ is $2/Tm$, or twice the width of the main lobe of $Q_o(f)$. Of course, for $Q_2(l')$ and $Q_3(l')$ the main lobe width is $2/L$. The <u>equivalent width</u> for these functions is investigated in detail by Blackman and Tukey with the final result that

3·7·1 $ERP_2(f) = ERP_3(f) \cong Tm$ for $Q_2(f)$, $Q_3(f)$

3·7·2 $ERP_2(1') = ERP_3(1') \cong L$ for $Q_2(1')$, $Q_3(1')$

Which is seen to be only half the resolving power obtained for i = o. Also, adjacent estimates of the spectral density function are not independent for the discrete spacing used in equations 2·24 and 2·25. Therefore, when using i = 2 or i = 3 spectrum window or array pattern every other spectral density estimate may be regarded as independent.

The resolving power given by equation 3·7 is a conservative one. The signal need not be strictly Gaussian nor the spectrum flat. The results apply so long as the signal is nearly Gaussian and the spectrum is slowly changing. If sharp transitions or lines appear in the spectrum the resolving power may be reduced by one half at those places.

Under most circumstances the advantage of using one particular modified truncating function over another is slight compared to the fact that all the modified truncating functions substantially reduce the distortion of the spectrum while at the same time they reduce the resolving power by a factor of about two. The modified truncating functions are commonly used to smooth frequency spectra where the effect of sampling variability can be partially removed by using these low resolution spectral windows. At the same time distortion is reduced and "impossible" negative values in the power spectrum which may appear as a result of the strong negative side lobes of the $Q_o(f)$ spectral window, are eliminated by the improved shape of modified spectral windows. On the other hand, if it is important to distinguish fine detail, rapid transitions, or "lines", in the spectrum, it may be advantageous to accept the distortion caused by the abruptly terminated truncating function in order to gain higher resolution.

The ideas which have been presented here are recognized to be far from precise, particularly as regards to directional resolution. However, it is hoped that the discussion provides at least a qualitative appreciation of the problem. Extensive quantitative investigation of this subject would be warranted if intensive investigation of directional spectra were to be undertaken.

Directional Resolution

In developing the directional spectrum it becomes necessary, finally, to introduce an explicit relationship between the wave number and wave frequency. The directional spectral density may be obtained from the two dimensional spectral density by the transformation

3·8 $$S(\phi,f) = S(1',f)\cdot k'(\omega)\cos\phi$$

$$S(\phi,f) = S(1',f)\cdot\frac{2\pi f^2}{g}\cos\phi$$

Calculating the directional spectral density for discrete value of $\phi = \phi_q$ amounts to scanning the true $S(\phi,f)$ spectral density with the array directional pattern, moving it through an angle equivalent to one half the main lobe width for each value of q. The discrete values of ϕ are obtained as follows.

Since

$$1'_q = k'(\omega)\sin\phi_q$$

and since

$$1'_q = q/2L \qquad \text{for } q = 0, \pm 1, \pm 2, \ldots R$$

it follows that

3·9 $$\phi_q = \arcsin\,(q/2Lk'(\omega))$$

Now, according to the results of the last section the main lobe width for a rectangular truncating function is

$$W_o(1') = \frac{1}{L}$$

and it was also shown that successive values of q were equivalent to a displacement along the 1' axis of one half the main lobe width. Consequently, the angular width of the main lobe is given by

3.10 $$W_o(\phi) = 2 \arcsin \frac{(\lambda(\omega))}{2L}$$

where the wave length, λ, has been introduced according to the relation

$$k'(\omega) = 1/\lambda(\omega)$$

The angular resolving power is given by

$$ERP_o(\phi) = 1/W_o(\phi) = 1/2 \cdot \arcsin (\lambda(\omega)/2L)$$

Evidently, the angular resolution falls off as wave length increases, until $\lambda(\omega) = 2L$, at which point the main lobe width becomes 180°. Since 1' has previously been restricted, because of aliasing, to the range $1' \geq 1/2\Delta\xi$ it can be seen that the range of wave lengths which can be investigated by an array is restricted by the elemental spacing of detectors and the total length of the array. The range of wave frequencies corresponding to the wave length range can be found by introducing the specific relationship between k and ω for deep water gravity waves. Hence for

$$k'(\omega) = 1/\lambda(\omega) = 2\pi f^2/g$$

and for the wave length range

3·11·1 $$2\Delta\xi \leq \lambda \leq 2L$$

the range of frequencies becomes

3·11·2 $$\sqrt{g/4\pi L} \leq f \leq \sqrt{g/4\pi\Delta\xi}$$

or in terms of wave number

3·11·3 $\quad \pi/L \leq k \leq \pi/\Delta\xi$

It should be noticed that the array directional pattern is periodic on the range $-\pi/2 \leq \phi \leq \pi/2$ so that the pattern repeats itself on the range $\pi/2 \leq \phi \leq -\pi/2$ as can be seen by Eq. 3·9. Consequently a gravity wave which has a velocity component in the direction opposite to the direction of the wind cannot be distinguished from a similar gravity wave with a velocity component in the direction of the wind. This effect may be thought of as a sort of angular aliasing as it is an inherent property of sampling the sea surface along a line in space. The physical model has included an assumption, however, that only those gravity waves with velocity components in the direction of the wind can grow in amplitude by extracting energy from the wind. Consequently angular aliasing from the range $\pi/2 \leq \phi \leq -\pi/2$ is assumed to be unimportant.

Optimum Array Design

It is worthwhile to examine the summation indicated in Equation 2·25 for its influence on resolution. Here the summation is carried out over the intervals $r\Delta\xi$ for r = 0, 1, ...R. Now since the observations at various points $x = r\Delta\xi$ consist of time averages, and since it has been assumed that the process $\{\zeta(x,t)\}$ is stationary in x it is not necessary for all of the intervals to have a common origin. In recognition of this fact Barber (1958) has described a method whereby a given number of detectors can be used to form an array of maximum length.

The advantage of his procedure lies in the fact that the angular resolving power is directly proportional to the length of the arrays as can be seen from equations 3·7·2. Furthermore the minimum spacing of detectors, $\Delta\xi$, is determined by considerations of aliasing. Therefore this procedure may be used to achieve maximum angular resolution with a minimum number of detectors, thus achieving an economy of instruments.

For K detectors Barber finds the optimum array length, L_B, to be

3·12 $$L_B = R_B \Delta\xi = [(\frac{K}{2} + 1)^2 - 3]\Delta\xi$$

where R_B is the optimum number of intervals of length $\Delta\xi$. If the K detectors had been uniformly spaced then only R_u intervals can be achieved. Where

3·13 $$L_u = R_u \Delta\xi = [K-1]\Delta\xi$$

For reasonable values of K ($K \geq 6$) the optimum spacing allows construction of arrays with more than twice the resolution of uniformly spaced arrays employing the same number of detectors.

The spacing of the detectors may be summarized by the following scheme.

1. Let there be K detectors.
2. Assume K is even
3. Let $Q = K\Delta\xi/2$
4. Starting with a detector at one end of the array and working, say, to the right, locate a second detector at a distance Q.
5. Locate additional detectors to the right of the second detector to form Q-1 intervals of length Q+1.
6. Locate the remaining detectors, to the right, to form Q-1 intervals of length $\Delta\xi$.
7. If K is odd there should be Q intervals of length Q+1 to the right of the second detector instead of Q-1 intervals.

Array plans for K = 2 thru K = 14 are shown in Figure 3·2.

Statistical Stability

It can be shown that for a slowly varying power spectrum arising from a Gaussian signal the statistical stability of each spectral density estimate may be given in terms of the chi-square distribution. The variability of each spectral density estimate may be given in terms of confidence limits when the number of degrees of freedom of the chi square distribution has been specified.

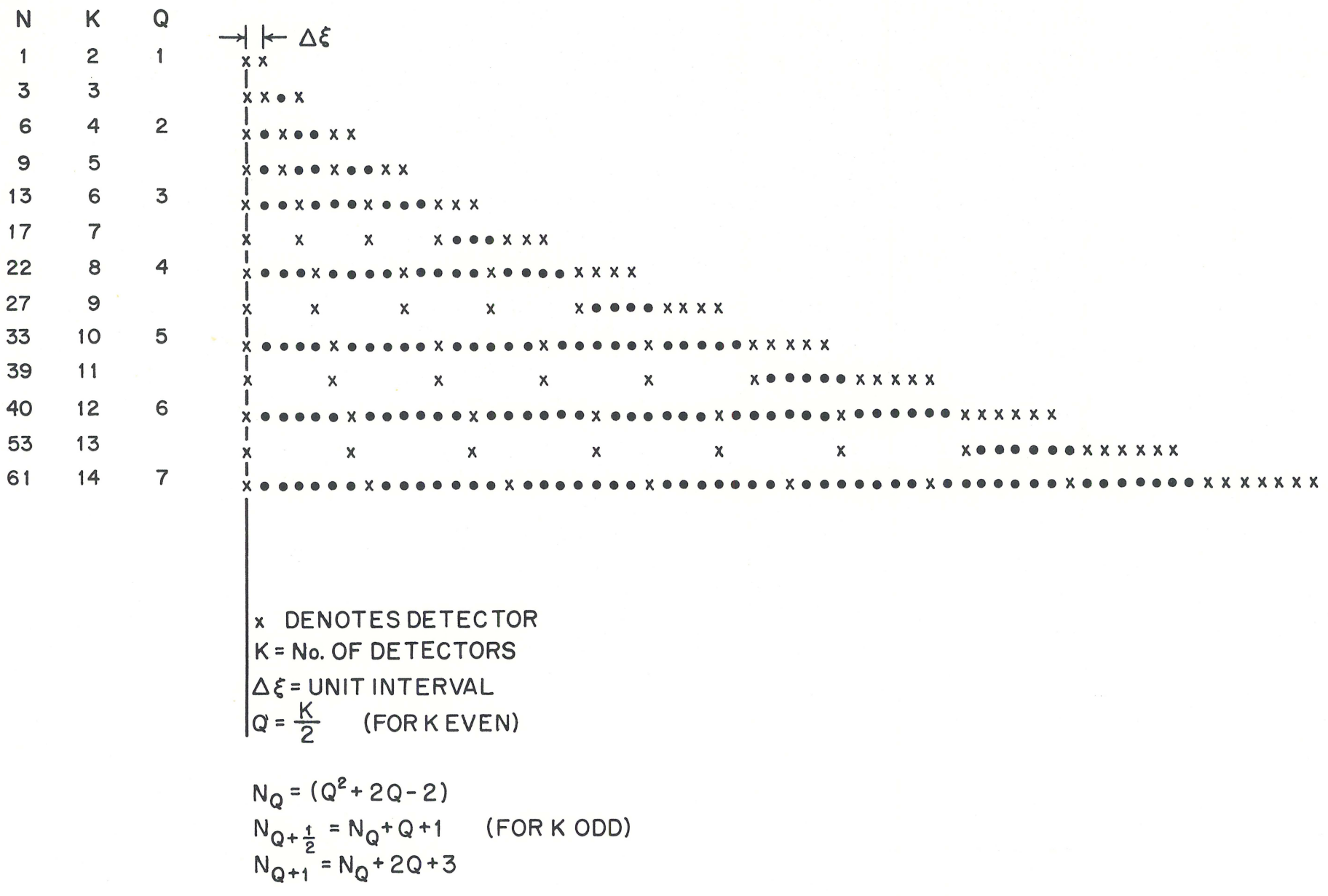

Fig. 3.2 Optimum array plans.

For power spectra Blackman and Tukey give

3·14 $$k_f = 2\ Tn'\ W_{ei}(f)$$

where k is degrees of freedom of the chi square distribution

Tn' = the effective length of the total record
$= Tn - Tm/3$
$W_{ei}(f)$ = equivalent width of the spectrum window

If $Q_3(f)$ is used, then $W_{ei}(f) = 1/Tm$ so that for the discrete parameter case

3·15 $$k_f = \frac{2(N-m/3)}{m}$$

The effective length of the time history is given by

3·16 $$Tn' = (N-m/3)\cdot\Delta t$$

and is an average of the actual number of data points entering into the sum

$$\sum_{i=1}^{N-p} \zeta_i(x)\cdot\zeta_{i+p}(x)$$

Unfortunately no such simple relationship exists for the co and quadrature spectra. The co and quadrature spectral density estimates will be statistically distributed according to a complex distribution which Goodman (1957) finds to be a complex analogue of the Wishart distribution.

The results, as developed by Goodman, do not provide an a-priori estimate of the statistical stability based on known parameters such as is the case for power spectra, but rather the calculated values of the co and quad spectra must be used, along with the coherency, in order to obtain stability estimates. Furthermore, the probability distribution of the

function, has not been tabulated; which means that the actual calculation of confidence levels would have to be carried out in order to obtain estimates of statistical stability.

Since the immediate objectives of the present work are only of an exploratory nature and since it is only intended to compare directional sea wave spectra with one another, no further investigation of the statistical stability will be attempted here. Instead, calculation of the various directional spectra will be carried out using the same number of observations for each of the spectra to be compared. Thus if the spectra to be compared do not differ too radically from one to another their statistical stability should be sensibly the same. Furthermore, a comparison of the stability of the power spectral density estimates from one case to the next should be indicative of any radical change in the stability of the directional spectral density estimates.

Computing Formulae

The pertinent formulae used in calculating the directional spectra will be given here in simplified notation. The equations for the cross covariance function may all be written in the form of Equation 3·17.

Here, "a", and "b" are the "names" of two series $\{a_n\}$ and $\{b_n\}$ whose values are given for $t = 0, \Delta t, 2\Delta t, \ldots, n\Delta t, \ldots, N\Delta t$. Notice that the summation index is now given over the range n-p to N instead of n to N-p. The calculations in this form depend only on the past history of the series and it becomes possible to introduce $\{a_n\}$ and $\{b_n\}$ into the calculations term by term as they would occur in real time.

If the series do not have zero means, the means may be extracted after calculating the sums of products, using the expression inside the square brackets of Eqn 3·17. This expression extracts a mean based only upon the terms which appear in each of the sums of products. It has been found useful to employ this method on smaller computers, though of course it is always preferable to extract the mean from the series terms prior to calculating the sums of products.

Covariance Function

$$3.17 \quad R_i(p:a,b) = \frac{D_i(p)}{N-p} \left\{ \sum_{n=1}^{N} a_{n-p} \cdot b_n - \left[\frac{1}{N-p} \sum_{n=1}^{N} a_{n-p} \cdot \sum_{n=p+1}^{N} b_n \right] \right\}$$

Where

$p=0,1,2 \cdots m \ll N$

$a_{n-p} = b_{n-p} \cong 0 \quad$ for $n-p \leq 0$

i denotes lag window $D_i(p)$

Cospectrum

$$3.18 \quad Sc_i(h:a,b) = \frac{2}{2m+1} \sum_{p=0}^{m} [R_i(p:a,b) + R_i(p:a,b)] \cdot \delta(p) \cdot \cos \frac{\pi p h}{m}$$

Quadrature Spectrum

$$3.19 \quad Sq_i(h:a,b) = \frac{2}{2m+1} \sum_{p=0}^{m} [R_i(p:a,b) - R_i(p:a,b)] \cos \frac{\pi p h}{m}$$

Where $h = 0,1,2, \cdots m$

$$\delta(p) = \begin{cases} 1 & \text{for } p = 1, 2, \cdots m-1 \\ 1/2 & \text{for } p = 0, m \end{cases}$$

i Denotes Spectrum Window Corresponding to Lag Window

Power Spectrum

$$3.20 \quad S_i(h:a) = Sc_i(h:a,a) \qquad \text{When } a = b$$

Normalized CoSpectrum

$$3.18.1 \quad U_i(h:a,b) = Sc_i(h:a,b) \cdot [S_i(h:a) \cdot S_i(h:b)]^{-1/2}$$

Normalized Quadrature Spectrum

$$3.19.1 \quad V_i(h:a,b) = Sq_i(h:a,b) \cdot [S_i(h:a) \cdot S_i(h:b)]^{-1/2}$$

Directional Spectrum

$$3.21 \quad S_{ij}(n:h) = \overline{S}(h) \cdot \frac{1}{2\pi} \cdot k(h) \cdot \cos(n\Delta\phi) \left\{ \sum_{r=0}^{R} U_i(h:r)\, \delta(r) \cdot D_j(r) \cdot \cos[r\Delta\xi \cdot k(h) \cdot \sin(n\Delta\phi)] + \sum_{r=0}^{R} V_i(h:r) \cdot D_j(r) \cdot \sin[r\Delta\xi \cdot k(h) \cdot \sin(n\Delta\phi)] \right.$$

Where

$n = 0, \pm 1, \pm 2, \cdots \pm Q \leq \pi/2\Delta\phi$

$k(h) = \frac{1}{g} (\pi h/\Delta tm)^2$

$$\delta(r) = \begin{cases} 1 & \text{for } r = 1, 2, \cdots R-1 \\ 1/2 & \text{for } r = 0, R \end{cases}$$

Subject to the Restriction that

$\pi/L \leq k(h) \leq \pi/\Delta\xi$

And

$n \leq \pi/2\Delta\phi$

Notice that the truncating function, or lag window, is shown as part of Eqn 3·17. In the case of the hanning or hamming lag windows it is possible to achieve the same effect by applying a three point smoothing after calculating the spectrum. This procedure may save some computer time though it is of little advantage even on moderate speed computers. Since other form of lag windows do not share this property it is more consistent to apply the lag window to the covariance calculation.

The computational forms for the co and quadrature spectra and power spectrum are given by Equations 3·18 through 3·20. These formulae differ from the comparable Equations 2·24 and 2·25 in the following respects:

1. The quantity to be calculated is the integral of the spectral density over the range Δf. This quantity will be called the power spectrum, cospectrum, quadrature spectrum or simply spectrum. It represents the contribution to the total variance due to a band of frequencies centered at f_n and of width Δf. The symbols appearing on the left hand side of Equations 3·18 through 3·20 are related to the comparable quantities of Equations 2·24 and 2·25 as:

$$Sc_i(h:a,b) = \{S_c(\xi,h)*Q_i(h)\}\Delta f$$

$$Sq_i(h:a,b) = \{S_q(\xi,h)*Q_i(h)\}\Delta f$$

$$S_i(h:a) = \{S_x(h)*Q_i(h)\}\Delta f$$

$$S_i(h:b) = \{S_\xi(h)*Q_i(h)\}\Delta f$$

2. The equations 3·18 through 3·20 are defined for positive frequencies ($h \geq 0$)only, so the spectral densities have been multiplied by two. Therefore, since $\Delta f = 1/Tm$, the coefficient on the right hand side becomes $2\cdot\Delta\tau\cdot\Delta f = 1/m$.

The notation for the co and quadrature spectra may be further simplified in the present case since if a and b denote a specific pair of detectors then there is an interval of length $r\Delta\xi$ associated with that pair. Therefore using r to denote a specific interval define the power spectrum, and the normalized co and quadrature spectrum for that interval as follows:

3·20·1 $S_i(h:r) = [S(h:a)\cdot S(h\cdot b)]^{1/2}$ power spectrum

3·18·2 $U_i(h:r) = Sc_i(h:a,b)/S_i(h:r)$ normalized cospectrum

3·19·2 $V_i(h:r) = Sq_i(h:a,b)/S_i(h:r)$ normalized quadrature spectrum

Define the <u>average power spectrum</u> to be

3·20·2 $$\overline{S(h)} = \frac{1}{R}\sum_{r=1}^{R} S_i(h:r)$$

Now, the directional spectrum may be expressed in terms of the normalized co and quad spectra and the average power spectrum, as is given in Equation 3·21.

The discussion in the preceding sections has shown that if the rectangular truncating function is used and if the signal is Gaussian with slowly varying spectrum, then spectral density estimates made at intervals of

$$\phi_q = \arcsin [q/2Lk'(\omega)]$$

will be statistically independent. However, it is neither essential nor desirable to evaluate the directional spectrum at these intervals. In fact in an exploratory analysis, such as is proposed here, it may be much more important to expose the detailed structure of the spectrum rather than attempt precise quantitative measurement. Therefore, the computational formula for the directional spectrum is given for arbitrary increments of ϕ.

It should be borne in mind that the maximum detail which can be observed by evaluating the directional spectrum at intervals closer than the resolving power of the array, will be a trace of the directional array pattern, itself. Even so, if an exact trace of the directional array pattern be observed the preceding discussion of directional resolution shows that the true spectrum could be anything from a single line to a rectangular spectrum half the width of the main lobe.

The calculated quantity in this case is the <u>directional spectrum</u> over the two dimensional interval $\Delta f \cdot \Delta\phi$. The symbol appearing on the left hand side of Equation 3.21 is defined in terms of Equation 2.25 as:

$$3.21 \qquad S_{ij}(n,h) \doteq \{\hat{S}(n,h) * Q_i(h) * Q_j(h)\} k \cos\phi \cdot \Delta\phi \cdot \Delta f$$

where the index n is used instead of q to indicate arbitrary choice of $\Delta\phi$.

Chapter IV Preliminary Results of Directional Spectra Calculations

In this chapter some directional spectra calculated from wave observations taken in Buzzards Bay, Mass. are presented. These results are given solely as a demonstration of the foregoing work. No physical interpretation of the results will be attempted at this time.

The data from which the directional spectra were calculated was obtained by Mr. Harlow G. Farmer, now of the Department of Oceanography, University of Washington, Seattle, Washington. The data acquisition system and an early version of the data reduction system is described by Farmer and Ketchum (1960) and also by Farmer (1963). A later version of the data reduction system which was actually employed in this work is described by Ketchum and Stevens (1961). The structural design of the instrument platform is described by Carver (1958).

The surface height transducers are simply lengths of stainless steel wire 0.015 inches in diameter suspended from a rotatable, horizontal boom. A small lead ball of about 3 pound weight was attached to the end of each wire about 20 feet below the water surface. This simple expedient proved highly satisfactory and no motion of the wires could be detected due to wind or wave action. A total of six surface height detectors were used, arranged according to the optimum plan shown in Fig. 3.5, with an elemental spacing of 1.5 feet, which makes the total length of the array 19.5 feet. The water surface acts essentially as a short circuit to the resistance wire, so that the electrical resistance of the exposed wire varies in response to the height of the water surface at the wire. The resistance wire is incorporated into an electrical bridge network, the output of which is an electrical analogue of the water surface height at a given point. One arm of the electrical bridge may be used to compensate for the low frequency changes in the water level caused by tides, so that the electrical output of the bridge is a measure of the height of wind generated waves only.

The weak signal from each electrical bridge is amplified and converted into a frequency modulated tone suitable for recording on magnetic tape. The magnetic tape recording will, when replayed, reproduce the original analogue voltage quite accurately. The reproduced signal from the several surface height transducers are sampled in rapid succession by an electronic switching circuit and each sampled voltage is converted into a binary digital number; the accuracy of this conversion being very high. The binary digital number is then made available for processing on an electronic digital computer. The

overall accuracy of the data acquisition system is probably better than ± 2%, which means that each of the digital numbers is correct to within those limits of accuracy.

A suite consisting of five separate runs taken on 12 August 1959 was chosen for this exploratory investigation. Each run consists of approximately 15 minutes of continuously recorded data from the six wave height detectors, a fast response cup anemometer (Stevens and Shodin (1962)) and a wind vane. The entire array was rotated so as to be normal to the wind direction for each run.

The suite of records chosen for this analysis is of particular interest since the first four runs show the development of the power spectrum and directional spectrum of wind generated waves in response to a slowly increasing wind velocity while the fifth run may show the effect of declining wind. No temporal wind record exists for Woods Hole or Buzzards Bay on this day except the recorded wind observations so that the full wind history is not known. Nonetheless, the development and possible decline of the wave spectrum is evident from a study of Figures 4.1 through 4.5, which show the power spectra for the various runs.

Sampling and Aliasing of Data

The power spectra were computed by sampling the signal from each detector 4 times per second and a total of 1000 samples was taken for each detector. The sampling rate corresponds to a folding frequency of 2 cycles per second. A preliminary examination of some of the records was made, sampling at the rate of 10 samples per second. Power spectra for these runs indicated that the spectrum decreased uniformly to a noise level of less tha 2% of the spectral peak at 2 cycles per second and continued to decrease slowly as the folding frequency of 5 cps was approached. The data reduction apparatus has a low pass filter cut off at 10 cps. Examination of the graphic record and the behavior of the spectrum make it seem unlikely that a spectral power peak would occur in the unexplored range between 5 and 10 cps. It was therefore assumed that aliasing would not result in important distortion of the spectrum if the folding frequency was taken at 2 cps, corresponding to 4 samples per second. It would, of course be preferable to incorporate filters with a lower frequency cut off in the data processing equipment commensurate with the sampling rate or, to use a faster sampling rate and apply a digital low pass filter to the sampled data. Since neither of these alternatives are practical with the presently available equipment the possibility

of aliasing errors must be accepted, although, for reasons given above, it is expected that these errors will be small.

The criterion to prevent wave number aliasing as given in Chapter II is

2.22 $$\Delta\xi \leq g(\Delta\theta)^2/\pi = g/4\pi f_N^2$$

Since the folding frequency corresponding to $\Delta t = 0.25$ seconds is $f_N = 2.00$ cps, it follows according to 2.22 that

$$\Delta\xi \leq .64 \text{ ft.}$$

The actual value chosen for $\Delta\xi$ was 1.5 ft. This choice was made, and the observations were made before the analysis described in Chapters 2 and 3 was carried out. Therefore, the directional spectra will be aliased for wave lengths less than 3 ft. This is an unfortunate situation, which could be avoided in future observations, and could have been overcome with the present observations if a large scale computer was used to apply digital low pass filtering to the sampled data. However, an examination of the power spectrum shows that the total power spectral densities are very small above h = 19, where the wave length is about three feet long. For this reason it is argued that aliasing is of small consequence in the directional spectra and should not substantially affect the results of the type exploratory investigation attempted here.

Calibration of Surface Height Detectors

Prior to each run the electronic circuitry was balanced and the sensitivity of each surface height sensor was adjusted and calibrated so that the wave present at the time would cause nearly full scale deflection of the FM recording channels. Unfortunately, this procedure led to some ambiquity in the absolute values of the wave heights. As will be seen from the power spectra, the sensitivity of the detectors for any given run were in very close agreement. Furthermore, there is reason to believe that the ration of sensitivities between pairs of runs is accurate and reliable. However, the absolute sensitivity of any one run is not known and cannot be determined. Consequently, the ordinates of the power spectra and directional spectra are given in terms of arbitrary units. This unfortunate

situation arose because of an oversight during the recording of data when inappropriate information was recorded in the log. This ambiguity could have been resolved if the aparatus were available for examination; however, the force of wind and waves, (with a possible assist from a fishing boat suspected of mooring to the structure) destroyed the observing platform and the instrument system during the fall of 1959. It may be reasonably assumed, however, that the sea waves have a significant height of about 1.4 feet for Run 1 and 2.0 feet for Run 3.

Statistical Stability of Power Spectrum Estimates

According to the discussion in Chapter 3, the statistical stability of the power spectral density estimates may be given in terms of confidence limits calculated from the chi-square distribution if the number of degrees of freedom can be estimated using Equation 3.15.

3.15 $$k_f = \frac{2(N-m/3}{m}$$

In the present case N = 1000 and m= 30, so that

$$k_f = 66$$

The upper 95% and lower 5% confidence limits corresponding to 66 degrees of freedom are respectively 1.2289 and 0.7848.

Figure 4.1 through 4.5 illustrates the power spectra for the five runs considered here. The spectral estimates as calculated from each of the six detectors is plotted, where it is possible to do so. The average value for all six detectors is also shown in the figures and the upper 95% and lower 5% confidence intervals are also shown. The confidence limits are calculated using 66 degrees of freedom but are plotted against the average spectrum value. While some of the calculated spectral densities fall outside the confidence limits, as might be expected, it is interesting to note that no single detector consistently exceeds the bounds. This may be taken to mean that the probability of consistent error between detectors is small.

The abscissa in the figures is given in terms of the parameter "h". Conversion to frequency, wave-length, wave velocity, etc. may be done with the use of Table II.

Directional Characteristics of the Array

The range of wave-lengths, frequencies and wave numbers that can be investigated by the array are determined by the unit spacing between detectors, and the total array length, using Eqn. 3.11. In the present case $\Delta\xi = 1.5$ ft. and $L = 19.5$ ft.

3.11.1	$3 \leq \lambda \leq 39$	ft.
3.11.2	$362.5 \leq f \leq 1306.5$	mcps
3.11.3	$0.161 \leq k \leq 2.094$	1/ft.

However, since the frequency spectra are only calculated for the discrete values $f_h = h/2\Delta t.m$ it is found that the range of the array is given in terms of "h" as

$$6 \leq h \leq 19$$

which corresponds to a frequency range of

$$400 \leq f_h \leq 1270 \qquad \text{mcps}$$

The actual shape of the directional array patterns at various values of "h" within the above range are shown in Figure 4.7.

Discussion of the Results of the Calculations

The suite of five runs selected for analysis are of particular interest since they show the development of the power spectrum and directional spectrum during the onset of a sea breeze. The wind increased during the first four runs and diminished slightly during the fifth run. The observations were taken on 12 August 1959 starting at 1225 hours. Each run consisted of a continuous record

of surface elevation from six wave height detectors, one anemometer and a wind vane.

Figure 4.6 shows a superposition of the power spectra for the five runs. The plotted lines correspond to the mean of the spectral densities measured by the six detectors. The abscissa is again given in terms of the parameter "h", which can be converted to various wave parameters with the aid of Table II. It is unfortunate that neither absolute values of the spectral densities nor a continuous wind velocity record are available since this information would permit some deductions about the rate of growth of the power spectrum.

The result of the directional spectra computations is summarized in Figure 4.7. An effort has been made to include as much pertinent information on the figure as possible. The first five vertical columns show the directional spectrum for each run as calculated at seven different values of "h" within the range of the array. The sixth column shows the form of the directional array pattern at the appropriate frequency. Though useful information is contained in the spectral estimates at all values of "h", the directional spectra are plotted only for the even values, in order to reduce the complexity of the illustration.

Various other means of presenting the data were studied prior to deciding on the format of Figure 4.7 as the most illustrative and compact. Since it was originally intended to present the data as a polar plot in k and ϕ the spectral densities S(1,f) were not multiplied by k upon converting them to the $S(\phi,f)$ densities. Furthermore, since the power spectrum ordinate was already in arbitrary units it was reasonable to plot only the normalized directional spectra. Therefore, the function shown in Figure 4.7 is, referring to Equation 3.21.

$$S_{3j}(n,h)/k\ \bar{S}(h) \qquad \text{for } j = 0,\ 3$$

the dark lines in the figure corresponding to $Q_o(\phi)$ and the light lines to $Q_3(\phi)$ directional array patterns. This presentation serves to illustrate the form of the directional spectrum and emphasizes its markedly line like structure, though care should be taken to appreciate the relatives magnitude of the spectrum at various frequencies by referring to Figure 4.6.

The calculation of the directional array pattern as shown in Figure 4.7 was done with the identical program used in calculating the other directional spectra. This was accomplished by generating data in the same format as the

actual cross spectra, having a power spectra and cospectrum of unit amplitude and quadrature spectum of zero amplitude at all frequencies: which is equivalent to a "white" frequency spectrum with wave fronts all parallel to the array. This procedure was followed in order to eliminate the possibility that the surprising structure of the directional spectrum was caused by an error in the directional spectrum program itself.

The elapsed time in minutes from the beginning of the first run, at 1225 on 12 August 1959 is noted above each column. Also shown is the mean wind velocity observed during the run. The wave parameters frequency (f), wave length (λ) and phase velocity (c) shown in the right margin of the figure correspond to the value of "h" shown in the left margin.

The unusual and surprising form of the observed directional spectra has been carefully considered. It was first supposed that the secondary peaks which begin to appear at h = 10, in some runs, were caused by the strong side lobes of the Q_o directional array pattern. In order to eliminate this possibility the spectra were recalculated using the directional array pattern Q_3, which minimizes the first side lobe. Since the peaks are still apparent under these circumstances they cannot be due to side lobes.

While no attempt has been made to assign statistical confidence limits to the directional spectral densities, because of the complex nature of the relevant statistical distribution, it is felt that the general form and shape of the calculated directional spectra is established with reasonable certainty because of the similar form of the spectra for the five runs. The results shown in Figure 4.7 may, therefore, be regarded with considerable confidence as representing the general nature of the directional spectrum of wind generated sea waves.

TABLE II

Wave Parameters In Terms of Computed Integer Values of "h"

Δt = 0.25 sec
m = 30

H	f(mcps)	T(sec)	w(rad/sec)	k(ft^{-1})	λ(ft)	c(ft/sec)
1	67	15.00	.42	.01	1151.65	76.78
2	133	7.50	.84	.02	287.91	38.39
3	200	5.00	1.26	.05	127.96	25.59
4	267	3.75	1.68	.09	71.98	19.19
5	334	3.00	2.09	.14	46.07	15.36
6	400	2.50	2.51	.20	31.99	12.80
7	467	2.14	2.93	.27	23.50	10.97
8	534	1.88	3.35	.35	17.99	9.60
9	600	1.67	3.77	.44	14.22	8.53
.0	667	1.50	4.19	.55	11.52	7.68
.1	734	1.36	4.61	.66	9.52	6.98
.2	800	1.25	5.03	.79	8.00	6.40
.3	867	1.15	5.45	.92	6.81	5.91
.4	934	1.07	5.86	1.07	5.88	5.48
.5	1000	1.00	6.28	1.23	5.12	5.12
.6	1067	.94	6.70	1.40	4.50	4.80
.7	1134	.88	7.12	1.58	3.98	4.52
.8	1201	.83	7.54	1.77	3.55	4.27
.9	1267	.79	7.96	1.97	3.19	4.04
20	1334	.75	8.38	2.18	2.88	3.84
21	1401	.71	8.80	2.41	2.61	3.66
22	1467	.68	9.22	2.64	2.38	3.49
23	1534	.65	9.63	2.89	2.18	3.34
24	1601	.63	10.05	3.14	2.00	3.20
25	1668	.60	10.47	3.41	1.84	3.07
26	1734	.58	10.89	3.69	1.70	2.95
27	1801	.56	11.31	3.98	1.58	2.84
28	1868	.54	11.73	4.28	1.47	2.74
29	1934	.52	12.15	4.59	1.37	2.65
30	2001	.50	12.57	4.91	1.28	2.56

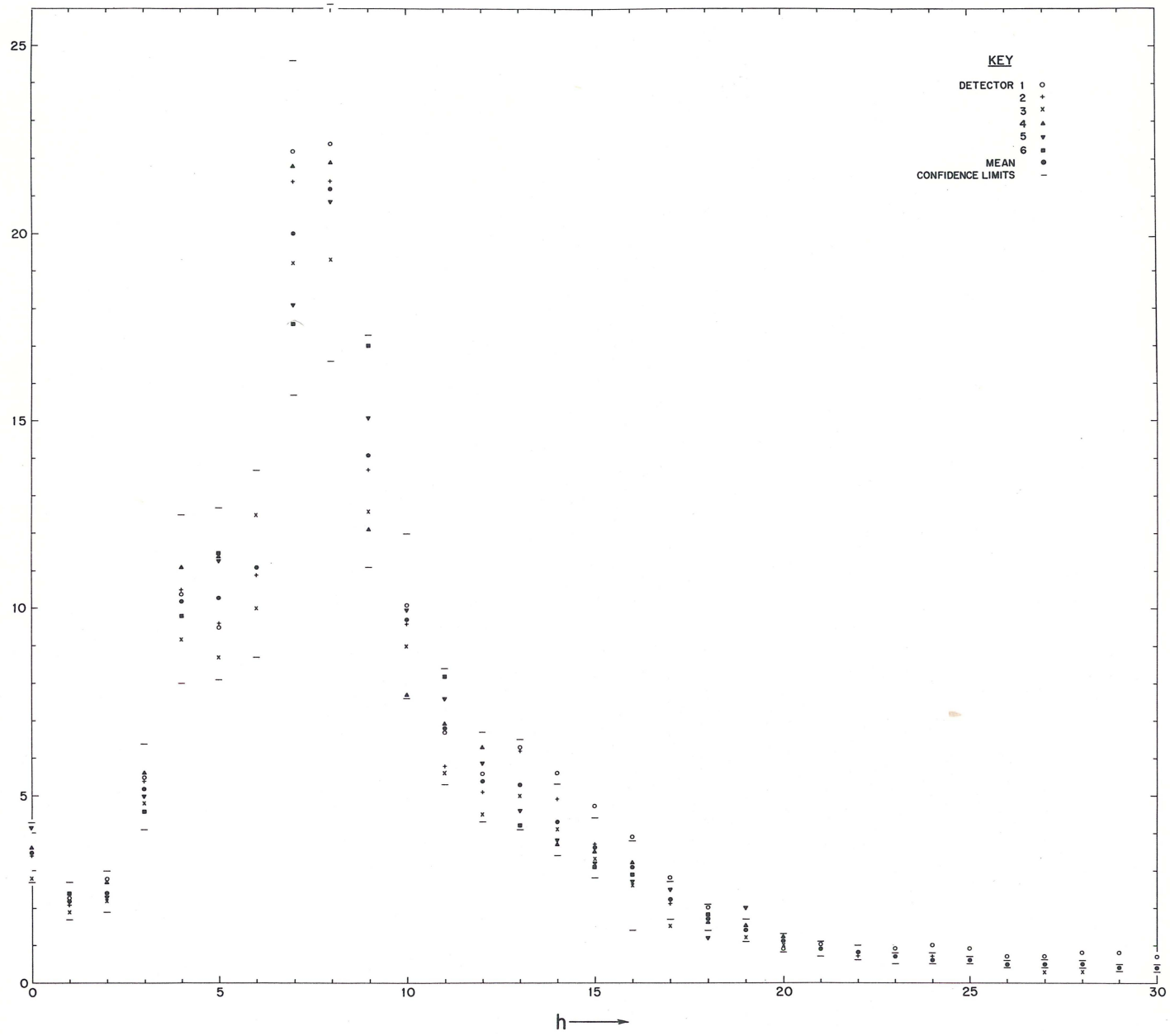

Fig. 4.1 Buzzards Bay Run 1 - power spectra as measured by six detectors and the 5% and 95% confidence limits.

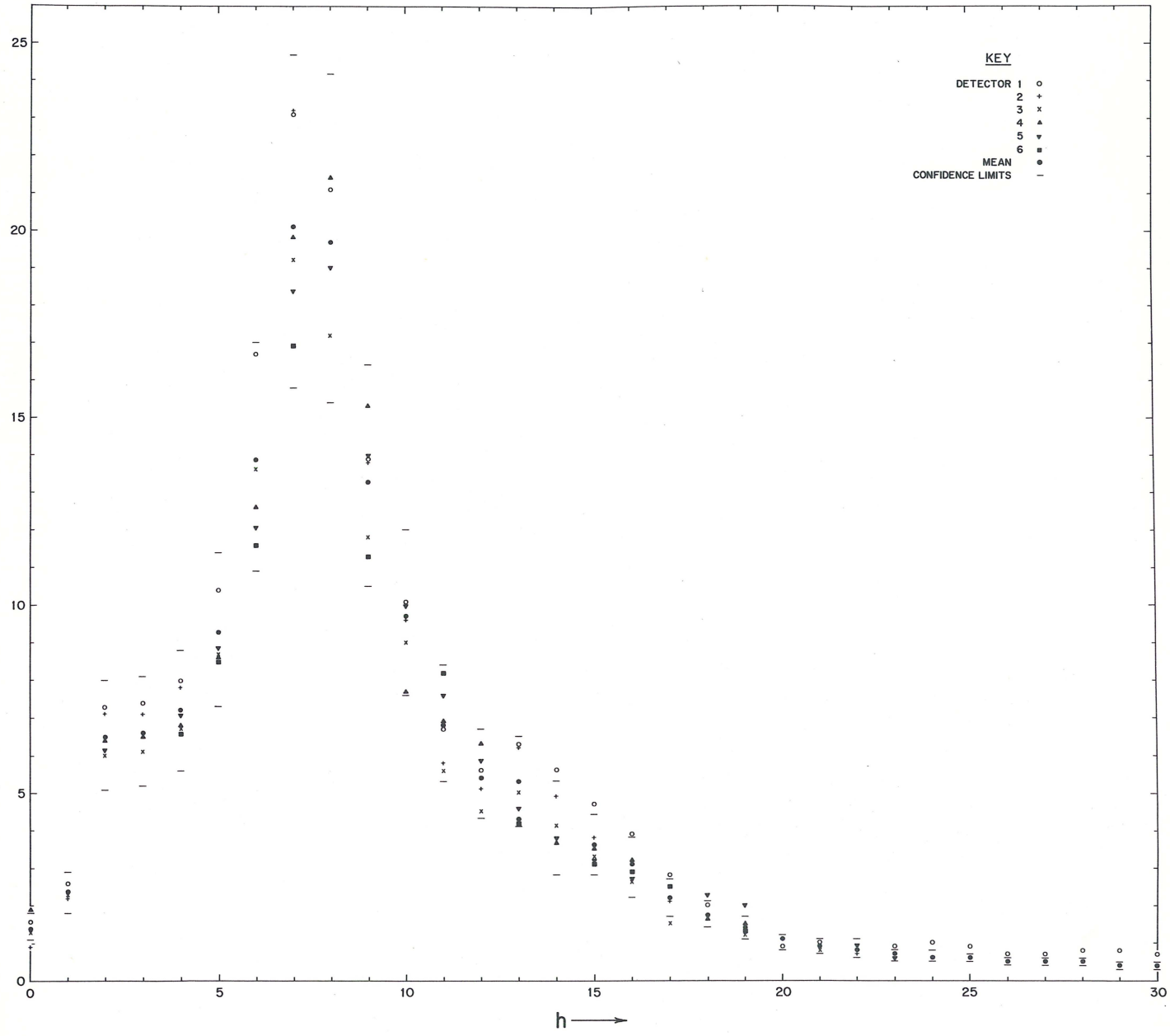

Fig. 4.2 Buzzards Bay Run 2 - power spectra as measured by six detectors and the 5% and 95% confidence limits.

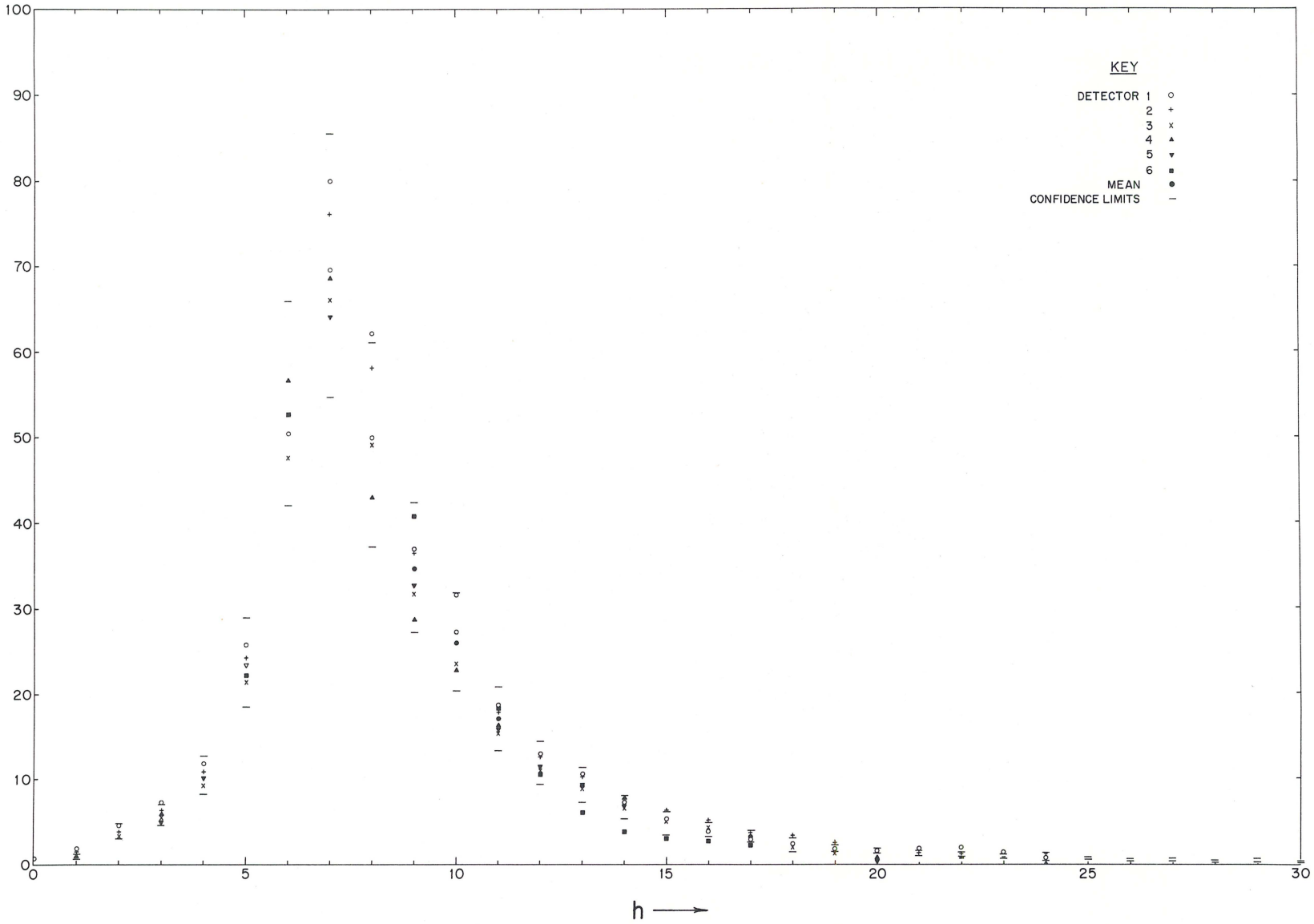

Fig. 4.3 Buzzards Bay Run 3 - power spectra as measured by six detectors and the 5% and 95% confidence limits.

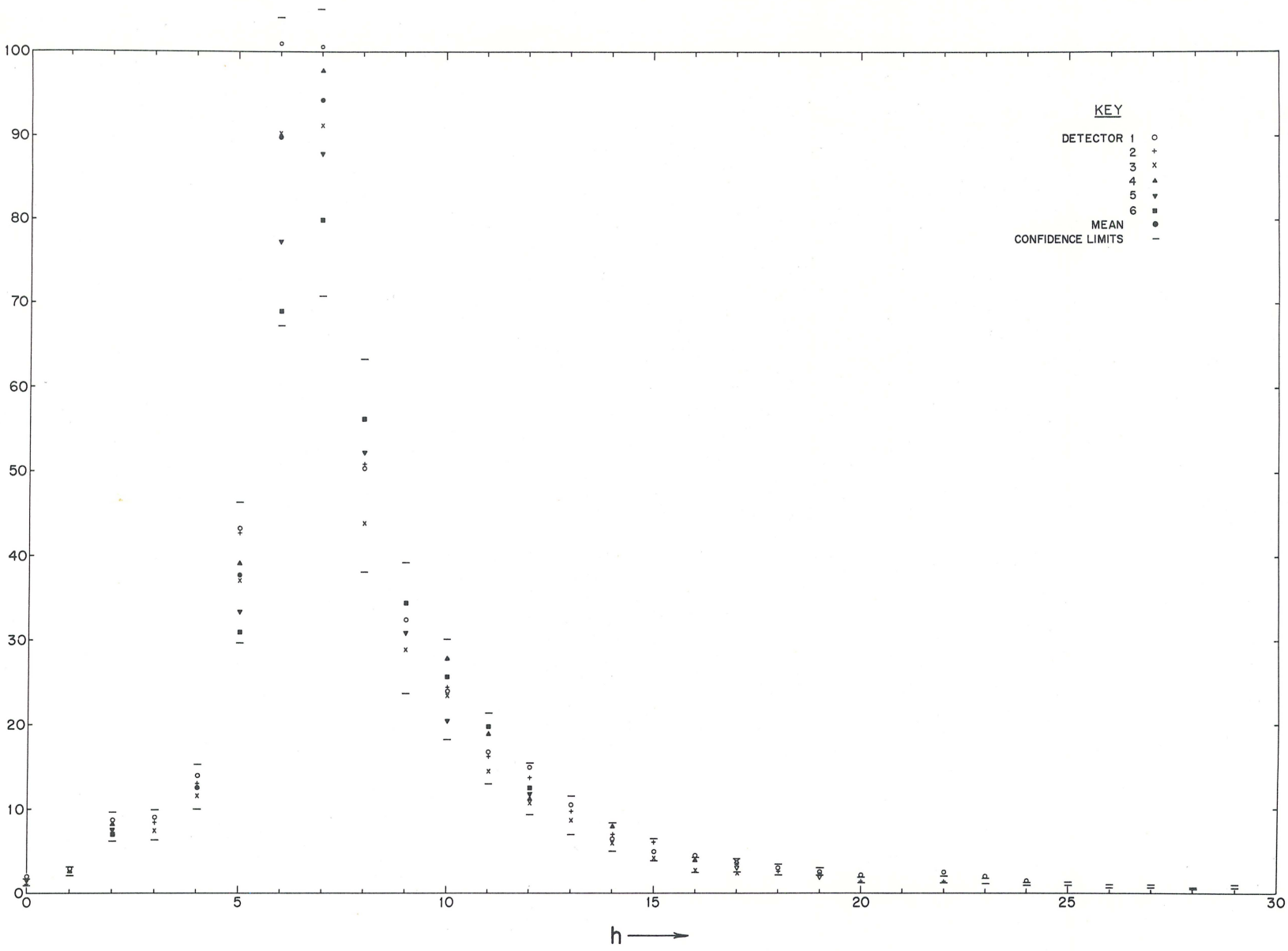

Fig. 4.4 Buzzards Bay Run 4 - power spectra as measured by six detectors and the 5% and 95% confidence limits.

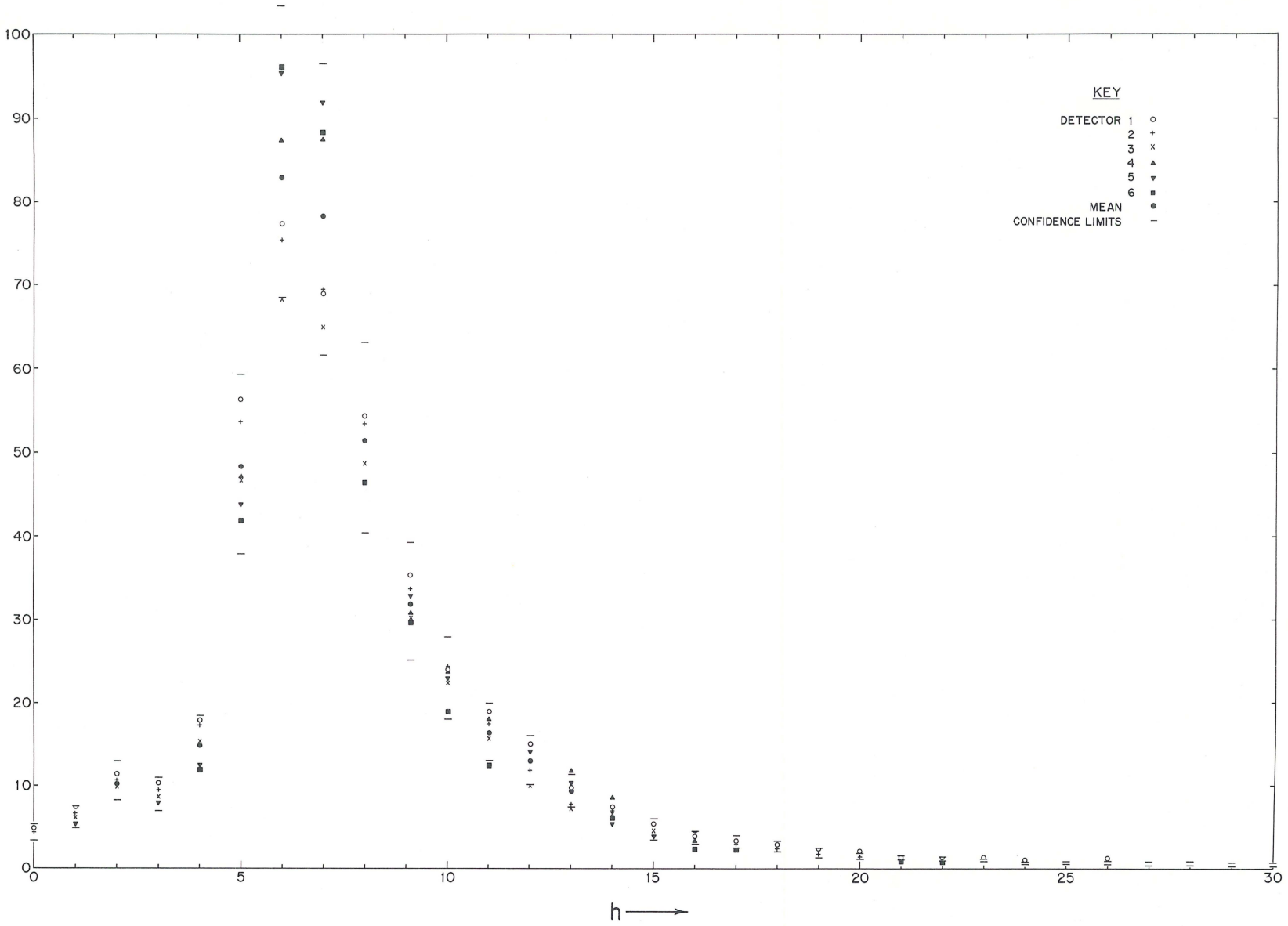

Fig. 4.5 Buzzards Bay Run 5 - power spectra as measured by six detectors and the 5% and 95% confidence limits.

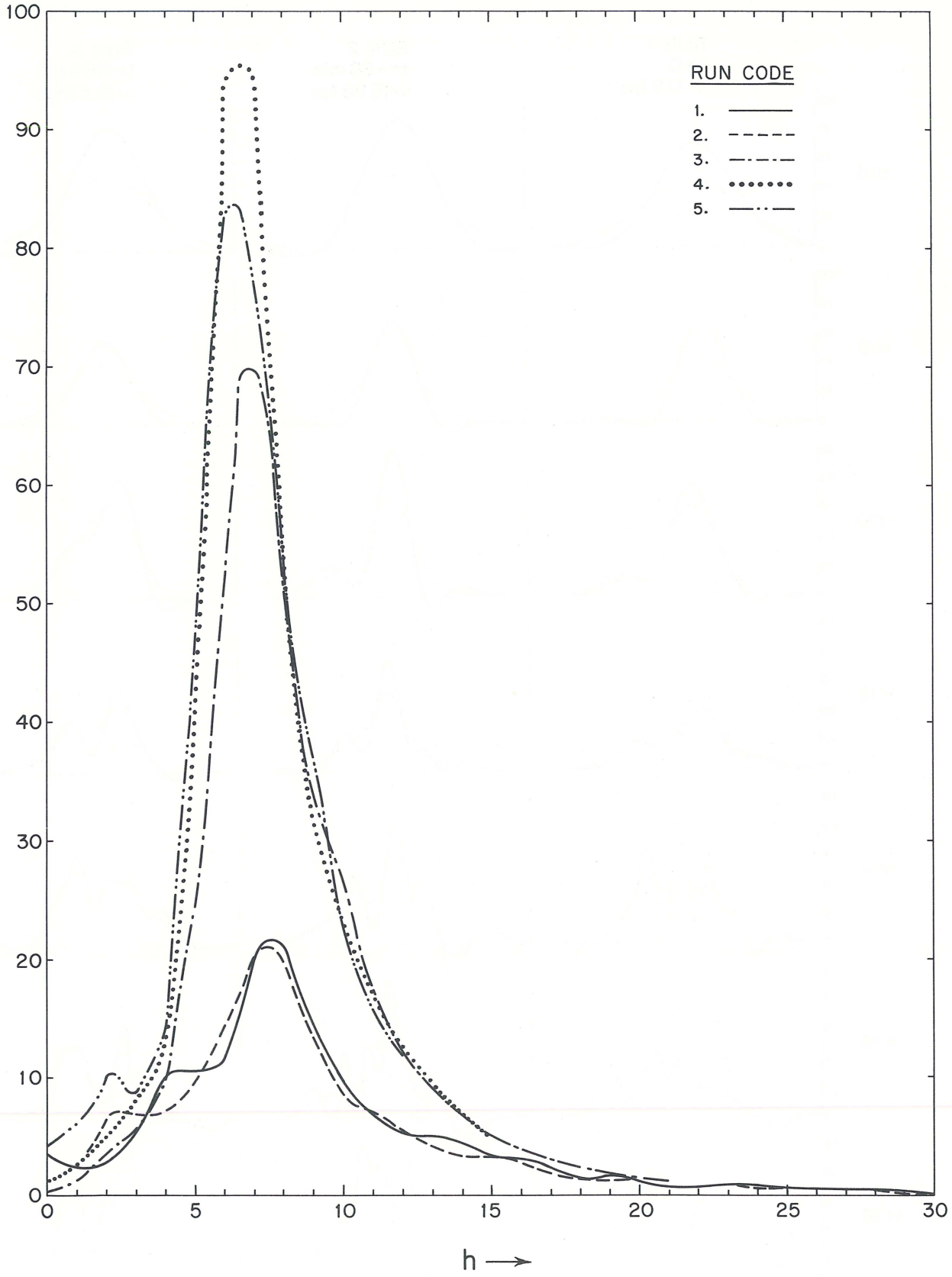

Fig. 4.6 Mean power spectra for Buzzards Bay Runs 1 through 5. Mean wind velocity: Run 1 - 11.90 feet per second, Run 2 - 15.98 fps, Run 3 - 18.53 fps, Run 4 - 20.23 fps and Run 5 - 18.70 fps.

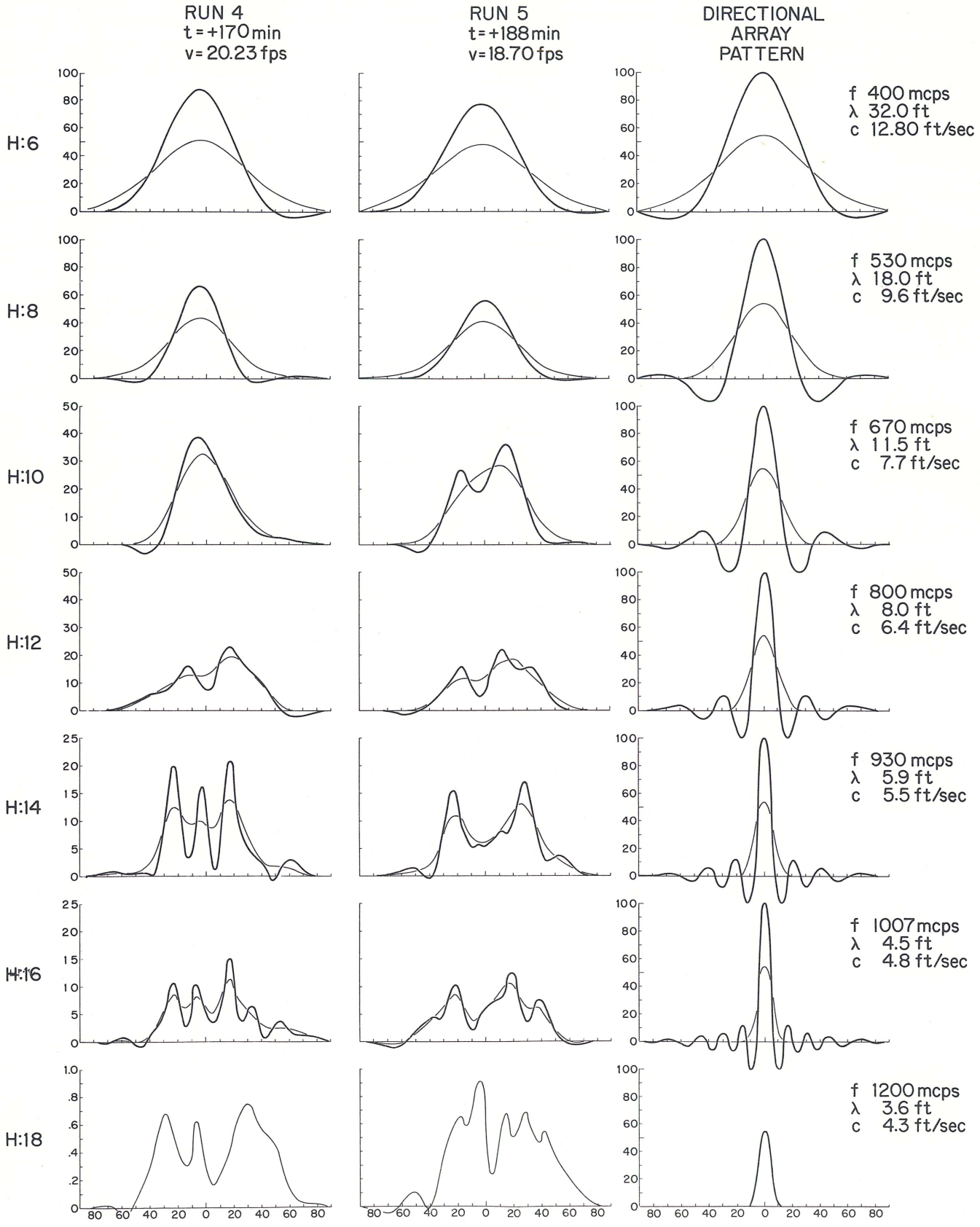

Fig. 4.7 Normalized directional spectra for Buzzards Bay Runs 1 through 5. Heavy lines are unsmoothed (Q_o) array pattern, light lines are smoothed (Q_3) array pattern.

References

Barber, N. F., (1958). Optimum Arrays for Direction Finding, N. F. Jour. Vol. 1, No. 1, 1958.

Barber, N. F., (1959). A Proposed Method of Surveying the Wave State of the Open Ocean, N. F. Jour. of Sci., Vol. 2, No. 1, 1959.

Barber, N. F., (1961). The directional Resolving Power of an Array of Wave Detectors. Proceedings of the Conference on Ocean Wave Spectra, Prentice-Hall, Inc., Englewood Cliffs, N. J. 1963.

Barber, N. F., (1961a). Experimental Correlograms and Fourier Transforms, Pergamman Press, New York 1961 (136pp).

Barber, N. F., (1962). Detecting Sea Waves by Their Diffraction of a Radio Wave, Technical Report Prepared for the Office of Naval Research, Woods Hole Oceanographic Institution, Ref. No. 62-39 (unpublished manuscript)

Barber, N. F. and Ursell, (1948). The Generation and Propogation of Ocean Waves and Swell. Phil. Trans. Toy. Soc., A 240, No. 824, 527-560.

Bendat, J. S., (1958). Principles and Applications of Random Noise Theory, John Wiley and Sons, New York 1958.

Blackman, R. B. and Tukey, J. W., (1958). The Measurement of Power Spectra from the Point of View of Communication Engineering. Dover Publications, Inc., New York (208pp).

Goodman, N. R., (1957). On the Joint Estimation of the Spectra, Cospectrum and Quadrature Spectrum of a Two Dimensional Stationary Gausnian Process. New York University College of Engineering, Engineering Statistics Laboratory, Scientific Paper No. 10.

Guillemin, E. A., (1949). The Mathematics of Circuit Analysis, John Wiley and Sons, New York 1949.

Hamming, R. W., (1962). Numerical Methods for Scientists and Engineers. McGraw Hill, New York 1962, (411pp).

Kinsman, Blair, (1960). Surface Waves at Short Fetches and Low Wind Speeds - a Field Study. The John Hopkins University, Chesapeake Bay Institute, Technical Report XIX, Reference 60-1.

Longuet-Higgins, M. S., (1957). The Statistical Analysis of a Random Moving Surface, Phil. Trans. Roy. Sve. A966V249, (pp 321-387).

Neuman, G. (1952). Über Die Komplexe Natur des Seeganges. I. Neve. Seegangsbeobachtungen in Nordatlantischen Ozean, Inder Karibschen See und in Golf in Mexico (M. S. Heidberg, Oct. 1950-Feb. 1951) Duet. Hydrog. Zeit 5, 95-110. II, Das Anwachsen der Wellen Unter Dem Einfluss des Windes. Deut. Hydrog. Zeit 5, 252-277.

Parzen, E. A., (1957). On Consistent Estimates of the Spectrum of a Stationary Time Series. Ann Mech. Stat. Vol. 28, (pp. 329-348).

Phillips, O. M., (1957). On the Dynamics of Unsteady Gravity Waves of Finite Amplitude, J. Fluid Mech. Vol. 3, Part 2, Nov. 1957.

Pierson, W. J., (Editor)(1960). The Directional Spectrum of a Wind Generated Sea as Determined from Data Obtained by the Stero Wave Observations Project, New York University, College of Engineering, Meteorological Papers, Vol. 2, No. 6, June 1960.

Pierson, W. J., (1961). Models of Random Seas Based on the Logranian Equations of Motion, New York University, College of Engineering, Technical Report Prepared for the Office of Naval Research (unpublished manuscript).

Pierson, W. J., Neumann G. and James, R. W., (1955). Observing and Forecasting Ocean Waves. U.S. Navy Hydro. Office, Publications No. 603.

DISTRIBUTION LIST

Unclassified Technical Reports for Oceanographic contractors of the Geophysics Branch of the Office of Naval Research (Code 416).

DEPARTMENT OF DEFENSE

1 Director of Defense Research and Engineering
Attn: Coordinating Committee on Science
Pentagon
Washington 25, D.C.

NAVY

2 Office of Naval Research
Geophysics Branch (Code 416)
Washington 25, D.C.

Office of Naval Research
Washington 25, D.C.
1 Attn: Biology Branch (Code 446)
1 Attn: Surface Branch (Code 463)
1 Attn: Undersea Warfare (Code 466)
1 Attn: Special Projects (Code 418)

1 Commanding Officer
Office of Naval Research Branch
495 Summer Street
Boston 10, Massachusetts

1 Commanding Officer
Office of Naval Research
207 West 24th Street
New York 11, New York

1 Commanding Officer
Office of Naval Research Branch
The John Crerar Library Building
86 East Randolph Street
Chicago 1, Illinois

1 Commanding Officer
Office of Naval Research Branch
1000 Geary Street
San Francisco 9, California

10 Commanding Officer
Office of Naval Research Branch
Navy #100, Fleet Post Office
New York, New York

1 Commanding Officer
Office of Naval Research Branch
1030 East Green Street
Pasadena 1, California

1 Oceanographer
Office of Naval Research Branch
Navy #100, Box 39
Fleet Post Office
New York, New York

1 Contract Administrator Southeastern Area
Office of Naval Research
2110 "G" Street, N. W.
Washington 7, D.C.

1 ONR Special Representative
c/o Hudson Laboratories
Columbia University
145 Palisade Street
Dobbs Ferry, New York

6 Director
Naval Research Laboratory
Attn: Code 5500
Washington 25, D.C.

(Note: 3 copies are forwarded by this addressee to the British Joint Services Staff for further distribution in England and Canada)

1 Oceanographer
U.S. Naval Oceanographic Office
Washington 25, D.C.
Attn: Library (Code 1640)

1 U.S. Naval Branch
Oceanographic Office
Navy 3923, Box 77
F. P.O.
San Francisco, California

Chief, Bureau of Naval Weapons
Department of the Navy
Washington 25, D.C.
1 Attn: FASS
1 Attn: RU-222

1 Office of the U.S. Naval Weather Service
U.S. Naval Station
Washington 25, D.C.

1 Chief, Bureau of Yards and Docks
Office of Research
Department of the Navy
Washington 25, D.C.
Attn: Code 70

Commanding Officer and Director
U.S. Navy Electronics Laboratory
San Diego 52, California
1 Attn: Code 2201
1 Attn: Code 2420

1 Commanding Officer and Director
U.S. Naval Civil Engineering Laboratory
Port Hueneme, California
Attn: Code L54

1 Code 3145
Box 7
P. Tugu Missile Range
Pt. Mugu, California

1 Commander, Naval Ordnance Laboratory
White Oak, Silver Spring, Maryland
Attn: E. Liberman, Librarian

Commanding Officer (Code 753)
Naval Ordnance Test Station
China Lake, California
1 Attn: Technical Library

1 Commanding Officer
Naval Radiological Defense Laboratory
San Francisco, California

Chief, Bureau of Ships
Department of the Navy
Washington 25, D.C.
1 Attn: Code 312
1 Attn: Code 341C
1 Attn: Code 631
1 Attn: Code 688

1 Officer in Charge
U.S. Navy Weather Research Facility
Naval Air Station, Bld. R-48
Norfolk, Virginia

1 Commander, U.S.N. Ordnance Test Station
Pasadena Annex
3202 East Foothill Boulevard
Pasadena 8, California
Attn: Pasadena Annex Library

1 U.S. Fleet Weather Facility
U.S. Naval Air Station
San Diego 35, California

1 Commanding Officer
U.S. Navy Air Development Center
Johnsville, Pennsylvania
Attn: NADC Library

1 Superintendent
U.S. Naval Academy
Annapolis, Maryland

2 Department of Meteorology and Oceanography
U.S. Naval Postgraduate School
Monterey, California

1 Captain B. H. Andrews, USN
Commanding Officer and Director
U.S. Navy Underwater Sound Laboratory
New London, Connecticut

1 Captain C. Blenman, Jr.
Commanding Officer
U.S. Naval Ordnance Test Station
China Lake, California

1 Captain J. H. Brandt, USN
Commanding Officer
U.S. Naval Underwater Ordnance Station
Newport, Rhode Island

1 Dr. R. J. Christensen
Technical Director
U.S. Navy Electronics Laboratory
San Diego 52, California

1 Captain R.E. Odening, USN
Commanding Officer
U.S. Naval Ordnance Laboratory
White Oak, Silver Spring, Maryland

1 Dr. Robert A. Frosch, Director
Hudson Laboratories
Columbia University
145 Palisade Street
Dobbs Ferry, New York

1 Mr. G.G. Gould
Technical Director
U.S. Naval Underwater Ordnance Station
Newport, Rhode Island

1 Dr. G.K. Hartmann
Technical Director
U.S. Naval Ordnance Laboratory
White Oak, Silver Spring, Maryland

1 Dr. J.E. Henderson, Director
Applied Physics Laboratory
University of Washington
1013 East 40th Street
Seattle 5, Washington

1 Captain H.C. Mason, USN
Commanding Officer and Director
U.S. Navy Electronics Laboratory
San Diego 52, California

1 Dr. J. W. Horton
Technical Director
U.S. Navy Underwater Sound Laboratory
New London, Connecticut

1 Dr. John C. Johnson
Director
Ordnance Research Laboratory
Pennsylvania State University
University Park, Pennsylvania

1 Captain A. E. Krapf, USN
Commanding Officer
U.S. Naval Research Laboratory
Washington 25, D.C.

1 Dr. Harry Krutter
Chief Scientist
U.S. Naval Air Development Center
Johnsville, Pennsylvania

1 Captain A.E. Paddock, U.S.N.
Commanding Officer
U.S. Naval Air Development Center
Johnsville, Pennsylvania

1 Dr. W. B. McLean
Technical Director
U.S. Naval Ordnance Test Station
China Lake, California

1 Captain J.A. Obermeyer, USN
Commanding Officer and Director
David Taylor Model Basin
Washington 7, D.C.

1 Dr. Karl E. Schoenherr
David Taylor Model Basin
Department of the Navy
Washington 7, D.C.

1 Mr. A. H. Schooley
Associate Director of Research
and Electronics
U.S. Naval Research Laboratory
Washington 25, D.C.

1 Dr. Fred N. Spiess, Director
Marine Physical Laboratory
University of California
San Diego 52, California

1 Dr. N. H. Jasper, Technical Director
U.S. Navy Mine Defense Laboratory
Panama City, Florida

1 Captain W. C. Bennett
Commanding Officer and Director
U.S. Navy Mine Defense Laboratory
Panama City, Florida

1 Dr. David Sternberg, Executive Secretary
Hudson Laboratories
Columbia University
145 Palisade Street
Dobbs Ferry, New York

1 Dr. S.J. Raff
Director Systems Analysis Group
U.S. Naval Ordnance Laboratory
White Oak, Silver Spring, Maryland

1 Dr. F. J. Weyl, Code 102
Office of Naval Research
Department of the Navy
Washington 25, D.C.

1 Dr. H. J. White
Office of Assistant Secretary
of the Navy (Research & Development)
Pentagon
Washington, D.C.

1 Captain W.T. Sawyer, Code 406
Office of Naval Research
Department of the Navy
Washington 25, D.C.

1 Dr. J.P. Craven, SP-001
Special Projects Office
Department of the Navy
Washington 25, D.C.

1 Dr. F.W. Loomis, SP-0051
Special Projects Office
Department of the Navy
Washington 25, D.C.

1 Mr. P. Waterman, Code 5360
U.S. Naval Research Laboratory
Department of the Navy
Washington 25, D.C.

1 Dr. T.E. Phipps
U.S. Naval Ordnance Test Station
China Lake, California

1 Mr. Robert A. Blaise
U.S. Naval Ordnance Test Station
China Lake, California

1 Mr. R.J. Miller
U.S. Naval Ordnance Laboratory
White Oaks, Maryland

1 Dr. D.F. Bleil
U.S. Naval Ordnance Laboratory
White Oaks, Maryland

1 Mr. W.C. Hodgson
U.S. Naval Research Laboratory
Department of the Navy
Washington 25, D.C.

1 Dr. W.H. Avery
Applied Physics Laboratory
Johns Hopkins University
8621 Georgia Avenue
Silver Spring, Maryland

1 Dr. W.F. Whitmore
Missiles Systems Division
Lockheed Aircraft Corporation
3251 Hanover Street
Palo Alto, California

1 Dr. E.S. Lamar, R-12
Bureau of Naval Weapons
Department of the Navy
Washington 25, D.C.

1 Captain F.A. Hooper, Code 330
Bureau of Ships
Department of the Navy
Washington 25, D.C.

1 Dr. G.C. Sponsler
Bureau of Ships
Department of the Navy
Washington 25, D.C.

1 Dr. T.C. Merkle
Lawrence Radiation Laboratory
Livermore, California

1 Dr. R.E. Williamson
Los Alamos Scientific Laboratory
Los Alamos, New Mexico

3 LCDR R. H. Yerbury
Executive Secretary
Special Projects Office (SP1142)
Department of the Navy
Washington, D.C.

AIR FORCE

1 Hdqtrs., Air Weather Service
(AWSS/TIPD)
U.S. Air Force
Scott Air Force Base, Illinois

1 ARCRL (CRZF)
L.G. Hanscom Field
Bedford, Massachusetts

ARMY

1 Army Research Office
Office of the Chief
of Research and Development
Department of the Army
Washington 25, D.C.

1 U.S. Army Beach Erosion Board
5201 Little Falls Road, N.W.
Washington 16, D.C.

1 Army Research Office
Washington 25, D.C.
Attn: Environmental Science Division

OTHER U.S. GOVERNMENT AGENCIES

1 Office of Technical Services
Department of Commerce
Washington 25, D.C.

10 Armed Services Technical
Information Agency
Arlington Hall Station
Arlington 12, Virginia

2 National Research Council
2101 Constitution Avenue
Washington 25, D.C.
Attn: Committee on Undersea Warfare
Attn: Committee on Oceanography

1 Commandant (OFU)
U.S. Coast Guard
Washington 25, D.C.

1 Commanding Officer
U.S. Coast Guard Oceanographic Unit
c/o Woods Hole Oceanographic Institution
Woods Hole, Massachusetts

1 Director
Coast and Geodetic Survey
U.S. Department of Commerce
Washington 25, D.C.
Attn: Office of Oceanography

1 U.S. Geological Survey
Washington 25, D.C.
Attn: James Trumbull

1 Director of Meteorological Research
U.S. Weather Bureau
Washington 25, D.C.

1 Director
U.S. Army Engineers Waterways
Experiment Station
Vicksburg, Mississippi
Attn: Research Center Library

1 Laboratory Director
Bureau of Commercial Fisheries
Biological Laboratory
450-B Jordan Hall
Stanford, California

Bureau of Commercial Fisheries
U.S. Fish and Wildlife Service
Post Office Box 3830
Honolulu 12, Hawaii
1 Attn: Librarian

1 Laboratory Director
Biological Laboratory
Bureau of Commercial Fisheries
P.O. Box 3098, Fort Crockett
Galveston, Texas

1 Laboratory Director
Biological Laboratory
Bureau of Commercial Fisheries
P.O. Box 6121, Pt. Loma Street
San Diego, California

1 Laboratory Director
Biological Laboratory; Auke Bay
Bureau of Commercial Fisheries
P.O. Box 1155
Juneau, Alaska

1 Laboratory Director
Biological Laboratory
Bureau of Commercial Fisheries
P.O. Box 6
Woods Hole, Massachusetts

1 Laboratory Director
Biological Laboratory
Bureau of Commercial Fisheries
P.O. Box 280
Brunswick, Georgia

1 Laboratory Director
Biological Laboratory
Bureau of Commercial Fisheries
P.O. Box 271
La Jolla, California

1 Bureau of Sport Fisheries and Wildlife
U.S. Fish and Wildlife Service
Sandy Hook Marine Laboratory
P.O. Box 428
Highlands, New Jersey
Attn: Librarian

1 Director
National Oceanographic Data Center
Washington 25, D.C.

2 Defence Research Member
Canadian Joint Staff
2450 Massachusetts Avenue, N.W.
Washington 8, D.C.

2 Library, U.S. Weather Bureau
Washington 25, D.C.

2 Director, Bureau of Commercial Fisheries
U.S. Fish and Wildlife Service
Department of Interior
Washington 25, D.C.

1 Director, Biological Laboratory
Bureau of Commercial Fisheries
Navy Yard Annex
Building 74
Washington 25, D.C.

1 Dr. Orlo E. Childs
U.S. Geological Survey
345 Middlefield Road
Menlo Park, California

1 Dr. John S. Schlee
U.S. Geological Survey
c/o Woods Hole Oceanographic Institution
Woods Hole, Massachusetts

1 Director
U.S. Navy SOFAR Station
APO 856
New York, New York

RESEARCH LABORATORIES

2 Director
Woods Hole Oceanographic Institution
Woods Hole, Massachusetts

3 ONR Scientific Liaison Officer
Woods Hole Oceanographic Institution
Woods Hole, Massachusetts

1 Director
Narragansett Marine Laboratory
University of Rhode Island
Kingston, Rhode Island

1 Bingham Oceanographic Laboratories
Yale University
New Haven, Connecticut

1 Gulf Coast Research Laboratory
Post Office Box
Ocean Springs, Mississippi
Attn: Librarian

1 Chairman
Department of Meteorology & Oceanography
New York University
New York 53, New York

1 Director
Lamont Geological Observatory
Torrey Cliff
Palisades, New York

1 Director
Hudson Laboratories
145 Palisades Street
Dobbs Ferry, New York

1 Great Lakes Research Division
Institute of Science & Technology
University of Michigan
Ann Arbor, Michigan
1 Attn: Dr. John C. Ayers

1 Dr. Harold Haskins
Rutgers University
New Brunswick, New Jersey

1 Director
Chesapeake Bay Institute
Johns Hopkins University
121 Maryland Hall
Baltimore 18, Maryland

1 Mail No. J-3009
The Martin Company
Baltimore 3, Maryland
Attn: J.D. Pierson

1 Mr. Henry D. Simmons, Chief
Estuaries Section
Waterways Experiment Station
Corps of Engineers
Vicksburg, Mississippi

1 Oceanographic Institute
Florida State University
Tallahassee, Florida

1 Director, Marine Laboratory
University of Miami
#1 Rickenbacker Causeway
Virginia Key
Miami 49, Florida

1 Nestor C. L. Granelli
Department of Geology
Columbia University
Palisades, New York

2 Head, Department of Oceanography
and Meteorology
Texas A and M College
College Station, Texas

1 Director
Scripps Institution of Oceanography
La Jolla, California

1 Allan Hancock Foundation
University Park
Los Angeles 7, California

1 Department of Engineering
University of California
Berkeley, California

1 Head, Department of Oceanography
Oregon State University
Corvallis, Oregon

1 Director
Arctic Research Laboratory
Barrow, Alaska

1 Dr. C. I. Beard
Boeing Scientific Research Laboratories
P.O. Box 3981
Seattle 24, Washington

1 Head, Department of Oceanography
University of Washington
Seattle 5, Washington

1 Geophysical Institute of the
University of Alaska
College, Alaska

1 Director
Bermuda Biological Station
for Research
St. Georges, Bermuda

1 Department of Meteorology
and Oceanography
University of Hawaii
Honolulu 14, Hawaii
Attn: Dr. H.M. Johnson

1 Technical Information Center, CU-201
Lockheed Missile and Space Division
3251 Hanover Street
Palo Alto, California

1 University of Pittsburgh
Environmental Sanitation
Department of Public Health Practice
Graduate School of Public Health
Pittsburgh 13, Pennsylvania

1 Director
Hawaiian Marine Laboratory
University of Hawaii
Honolulu, Hawaii

1 Dr. F. B. Berger
General Precision Laboratory
Pleasantville, New York

1 Mr. J.A. Gast
Wildlife Building
Humboldt State College
Arcata, California

1 Department of Geodesy and Geophysics
Cambridge University
Cambridge, England

1 Applied Physics Laboratory
University of Washington
1013 NE Fortieth Street
Seattle 5, Washington

1 Documents Division - ml
University of Illinois Library
Urbana, Illinois

1 Director
Ocean Research Institute
U. of Tokyo
Tokyo, Japan

1 Marine Biological Association
of the United Kingdom
The Laboratory
Citadel Hill
Plymouth, England

1 ASW Information Research Unit
Building 80, Plant A-1
Lockheed-California Company
Burbank, California

1 Advanced Research Projects Agency
Attn: Nuclear Test Detection Office
The Pentagon
Washington 25, D.C.

1 New Zealand Oceanographic Institute
Dept. of Scientific and Industrial Research
P.O. Box 8009
Wellington, New Zealand
Attn: Librarian

1 President
Osservatorio Geofisico Sperimentale
Trieste

1 Director
Defense Research Laboratory
The University of Texas
P.O. Box 8029
University Station
Austin 12, Texas

1 Chemistry Department
College of Engineering
University of Wisconsin
Madison 6, Wisconsin

National Institute of Oceanography
Mr. D. W. Privett, Librarian
Wormley
Godalming, Surrey,
England

Woods Hole Oceanographic Institution
Reference No. 63-22

On the Estimation of the Directional Spectrum of Ocean Waves from Time Series Observations of Surface Elevations.

Unclassified

This report attempts to present an overall account of a procedure used in calculating the directional spectrum of ocean waves. A simplified physical model is developed and used as the basis for the mathematical model. Some aspects of power spectrum and cross spectrum analysis are discussed in detail. Finally, some directional spectra calculations from data taken in Buzzards Bay Massachusetts are presented.

1. Directional Spectrum of Ocean Waves
2. Power Spectrum Analysis
3. Cross Spectrum Analysis

This card is UNCLASSIFIED

Woods Hole Oceanographic Institution
Reference No. 63-22

On the Estimation of the Directional Spectrum of Ocean Waves from Time Series Observations of Surface Elevations.

Unclassified

This report attempts to present an overall account of a procedure used in calculating the directional spectrum of ocean waves. A simplified physical model is developed and used as the basis for the mathematical model. Some aspects of power spectrum and cross spectrum analysis are discussed in detail. Finally, some directional spectra calculations from data taken in Buzzards Bay Massachusetts are presented.

1. Directional Spectrum of Ocean Waves
2. Power Spectrum Analysis
3. Cross Spectrum Analysis

This card is UNCLASSIFIED

Woods Hole Oceanographic Institution
Reference No. 63-22

On the Estimation of the Directional Spectrum of Ocean Waves from Time Series Observations of Surface Elevations.

Unclassified

This report attempts to present an overall account of a procedure used in calculating the directional spectrum of ocean waves. A simplified physical model is developed and used as the basis for the mathematical model. Some aspects of power spectrum and cross spectrum analysis are discussed in detail. Finally, some directional spectra calculations from data taken in Buzzards Bay Massachusetts are presented.

1. Directional Spectrum of Ocean Waves
2. Power Spectrum Analysis
3. Cross Spectrum Analysis

This card is UNCLASSIFIED

Woods Hole Oceanographic Institution
Reference No. 63-22

On the Estimation of the Directional Spectrum of Ocean Waves from Time Series Observations of Surface Elevations.

Unclassified

This report attempts to present an overall account of a procedure used in calculating the directional spectrum of ocean waves. A simplified physical model is developed and used as the basis for the mathematical model. Some aspects of power spectrum and cross spectrum analysis are discussed in detail. Finally, some directional spectra calculations from data taken in Buzzards Bay Massachusetts are presented.

1. Directional Spectrum of Ocean Waves
2. Power Spectrum Analysis
3. Cross Spectrum Analysis

This card is UNCLASSIFIED